Title
INFLUENCE OF HEAT TREATMENT ON THE FATIGUE CRACK GROWTH RATES OF A SECONDARY HARDENING STEEL

Author
Horn, R.M.

Publication Date
1973-08-01

Submitted to Metallurgical Transactions

LBL-2239
Preprint

INFLUENCE OF HEAT TREATMENT ON THE FATIGUE CRACK GROWTH RATES OF A SECONDARY HARDENING STEEL

R. M. Horn

August 1973

Prepared for the U. S. Energy Research and Development Administration under Contract W-7405-ENG-48

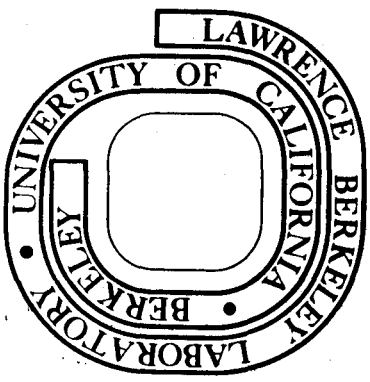

DISCLAIMER

INFLUENCE OF HEAT TREATMENT ON THE FATIGUE CRACK GROWTH RATES OF A SECONDARY HARDENING STEEL

R. M. Horn

Inorganic Materials Research Division, Lawrence Berkeley Laboratory and Department of Materials Science and Engineering, College of Engineering; University of California, Berkeley, California 94720

ABSTRACT

The relationships between microstructure and fatigue crack propagation behavior were studied in a 5Mo-0.3C steel. Microstructural differences were achieved by varying the tempering treatment. The amounts, distribution, and types of carbides present were influenced by the tempering temperature. Optical metallography and transmission electron microscopy were used to characterize the microstructures. Fatigue fracture surfaces were studied by scanning electron microscopy. For each heat treatment the fatigue crack growth properties were measured under plane strain conditions using a compact tension fracture toughness specimen. The properties were reported using the empirical relation of Paris [$da/dN = C_o \Delta K^m$]. It was found that secondary hardening did influence the fatigue crack growth rates. In particular, intergranular modes of fracture during fatigue led to exaggerated fatigue crack growth rates for the tempering treatment producing peak hardness. Limited testing in a dry argon atmosphere showed that the sensitivity of fatigue crack growth rates to environment changed with heat treatment.

INTRODUCTION

Fatigue crack propagation behavior is very important in determining the usefulness of high strength steels when they are subjected to cyclic loading. The crack initiation period, which adds significantly to the life in conventional fatigue studies, is often absent in the high strength materials because of pre-existing flaws, such as inclusions. Because of its successful use in predicting fracture conditions under static loading, linear elastic fracture mechanics has been applied to crack propagation. Paris and his colleagues[1,2] have proposed an empirical equation relating the stress intensity, K, to crack growth rate. They showed that the growth rate was related to the stress intensity range in the vicinity of the crack tip. Their relation is

$$\frac{da}{dN} = C_o(\Delta K)^m$$

where $\frac{da}{dN}$ is the change in crack length per cycle of loading, ΔK is the range of stress intensity being applied during cyclic loading, and C_o and m are experimental constants. This relation has been used to characterize the behavior of many materials;[3-6] investigations of the influence of steel purity and environmental effects have included it.[7,8] Some investigations have shown that specimen thickness can change fatigue crack propagation rates;[9] the effect of tempering temperature on crack growth has also been studied.[10,11] Relatively few attempts have been made to relate the microstructural changes associated with tempering to fatigue crack growth behavior, however.

Previous fracture toughness work has shown that large variations in toughness at equivalent yield strength levels occur in a quenched

and tempered 5Mo-0.3C secondary hardening steel.[12] The microstructural changes resulting from different tempering treatments have been characterized by transmission electron microscopy and used to explain the observed variation in fracture toughness. The present study was designed to determine the fatigue crack propagation behavior of the previously characterized 5Mo-0.3C steel in an ambient environment. A second objective was to determine how the microstructural features that control fracture toughness and tensile properties affect the fatigue crack growth behavior. The final objective was to ascertain what effect a dry environment had on fatigue crack growth rates in this steel.

EXPERIMENTAL PROCEDURES

Four 20 lb (9 kg) vacuum melted ingots were used in this study. The compositions are given in Table I. Each ingot was homogenized at 1100°C into bars 2 3/4 in. (70 mm) wide and 5/8 in. (15.9 mm) thick. Tensile and fracture toughness specimens were cut from the rolled bars, annealed at 1200°C for 1 hr in an argon atmosphere, ice-brine quenched, and refrigerated in liquid nitrogen to obtain a fully martensitic structure. Quenched specimens tempered for 1 hr in salt baths at 225°C, 300°C, 500°C and 600°C and air cooled were also tested.

Compact tension fracture toughness specimens meeting ASTM specifications[13] were used for the fatigue tests. All specimens were 9/16 in. (14.3 mm) thick to ensure plane strain conditions. Standard 1/4 in. (6.4 mm) round tensile specimens of 1 in. (25.4 mm) gage with threaded ends were used to measure tensile properties.

Fatigue tests were carried out at room temperature (20-25°C) in air (45-55% relative humidity) using a 300 KIP (1.33 MN) capacity MTS machine. Two additional tests in dry, room temperature argon were also conducted to evaluate the effect of moisture in the air environment tests. The specimens were tested at a frequency of 6 Hz under sinusoidal tension-tension cycling. Fatigue crack advancement was measured optically using a traveling microscope. Increases in crack advancement of 0.001 in. (0.025 mm) could be measured on the pre-polished specimen. The crack advancement, Δa, was measured on both surfaces of the specimen, and an average was used. The load was monitored continuously, and the tests were carried out using a minimum to maximum load ratio of $R = 0.11$ (where $R = P_{max}/P_{min}$). Because the minimum and maximum loads were kept

constant, the stress intensity range increased as the crack length increased. The formulation of the stress intensity for the compact tension specimen used is as follows:[13]

$$K_I = \frac{P}{W^{1/2}B} \cdot \left(29.6\left(\frac{a}{w}\right)^{1/2} - 185.5\left(\frac{a}{w}\right)^{3/2} + 655.7\left(\frac{a}{w}\right)^{5/2} - 1017.0\left(\frac{a}{w}\right)^{7/2} + 638.9\left(\frac{a}{w}\right)^{9/2}\right)$$

Because the stress intensity range increased, many data points were collected for each specimen. Cyclic loading was stopped and fracture toughness tests were carried out when $\frac{a}{w}$ reached about 0.7.

Fracture surfaces of the fatigue specimens were examined in a JEOLCO-JSM-U3 scanning electron microscope. Specimens cut from the fatigue specimen were used for metallographic examination. These specimens were mechanically polished and etched with a 5% nital solution. Transmission electron microscopy from an earlier study was also used for microstructure characterization.[12]

RESULTS AND DISCUSSION

Influence of Tempering Temperature on Strength and Toughness

The variations of the room temperature yield strength and plane strain fracture toughness behavior with tempering treatment are shown in Figs. 1(a) and 1(b). There was an increase in yield strength with tempering temperature in the neighborhood of 600°C, where a peak in hardness and yield strength occurred, as shown in Fig. 1(a). The fracture toughness dropped significantly where tempering temperatures greater than 225°C were used, as shown in Fig. 1(b). The lowest value (tempering temperature of 600°C) was approximately the same as that reported by Goolsby.[12]

Effect of Microstructural Features on Crack Propagation

The Paris relation[1] was used as a basis for analyzing the room temperature fatigue crack growth data. A least-squares log-log fit[14] line was used to determine the parameters in the empirical relation, as shown in Figs. 2(a) through (e). Duplicate tests were made for all tempering temperatures except the 600°C treatment. The results of the tests are shown in Figs. 2(a) through (e). Dry argon fatigue tests from single specimens for the as-quenched and 600°C treatment were also carried out. The results of these tests are shown in Figs. 3(a) and 3(b).

The following discussion is concerned with the relationships between the differences in microstructural features and the mechanical properties of steel. The effect of environment-microstructure interaction is subsequently discussed for two treatments, the as-quenched and 600°C tempering treatments, which yielded extremes in fatigue crack growth properties.

Microstructure and Crack Growth Rates of the As-Quenched Steel

Figure 4 is an optical photomicrograph showing the martensitic structure present in the as-quenched material. The large austenite grain size, 300-400 μm diameter, is apparent. As shown by transmission electron microscopy in Fig. 5, extensive autotempering was present in the martensite laths,[12] having occurred because the M_s temperature was high (about 425°C). The high M_s of the material was a consequence of the relatively low carbon content (0.3%) and the high austenitizing temperature. Goolsby has shown,[12] using dark field transmission electron microscopy, that the only carbide present in the autotempered martensite was cementite. No epsilon carbide was detected. The martensite was predominantly the dislocated lath type, which is characteristic of steels of this carbon content.[15] Internal twinning was observed only in isolated regions.

Figure 6 is a composite scanning electron micrograph of the fatigue fracture. The ΔK level in the area shown was 35 ksi-in.$^{1/2}$ (38 MN/m$^{3/2}$). The macroscopically measured crack growth rate at this ΔK was 1.5×10^{-5} in./cycle (3.8×10^{-4} mm/cycle). Features characteristic of quasi-cleavage were observed periodically in the fatigue area. An example of this is shown in the fatigue area in Fig. 6 at point A. This quasi-cleavage fracture may account for the scatter in some data points. Surrounding the quasi-cleavage area, A in Fig. 6, is evidence of localized plastic instability (at B). The diffuse markings resembling striations (at B) also suggest that the fatigue crack was not confined to a single plane. At C in Fig. 6, indications of striations are also seen. Striations are revealed more clearly in Fig. 7, which is a scanning electron

micrograph of another area where the ΔK was 40 ksi-in.$^{1/2}$ (43.5 MN/m$^{3/2}$). The measured average microscopic spacing of these striations 1.6×10^{-5} in. (4.0×10^{-4} mm) was approximately equal to the macroscopically measured crack growth rate 1.8×10^{-5} in./cycle (4.6×10^{-4} mm/cycle). The growth properties were associated with a microstructure characterized by autotempered laths of predominantly dislocated martensite. The fatigue crack growth associated with this microstructure followed an approximate second power dependence (m = 2.05) as shown by Fig. 2(a).

The excellent strength and fracture toughness properties of the steel in the as-quenched condition were attributed to the relatively uniform microstructure, characterized by dislocated autotempered martensite. No residual carbides or extensive lath boundary precipitation products were observed in the transmission studies. The yield strength of the as-quenched material was over 200,000 psi (1380 MN/m^2), and the fracture toughness was about 90 ksi-in.$^{1/2}$ (97 MN/m$^{3/2}$).

Figure 8 shows the fatigue crack propagation rates of the as-quenched 5Mo-0.3C steel along with crack growth rates for other quenched and tempered steels having yield strengths of about 200,000 psi (1380 MN/m^2).[7,9,11,16] As the figure shows, the as-quenched 5Mo-0.3C steel displayed fatigue crack propagation rates at high values of ΔK that were appreciably less than those reported for the other steels.

Microstructure and Fatigue Crack Growth Rates After Tempering at 225°C

Tempering at 225°C resulted in a significant increase in fracture toughness, as shown in Fig. 1(b), and a drop in yield strength, as shown in Fig. 1(a). Transmission electron microscopy revealed no obvious differences in microstructure between the as-quenched condition and the 225°C temper,[12] although the lower yield strength reflected the tempering of the martensite formed at lower temperatures during initial quenching.

The fatigue crack growth rates in the tempered samples were also characterized by a second power law ($m = 1.9$); the growth rates for a given ΔK were essentially the same as those for the as-quenched specimens. The appearance of the fatigue fracture surface was the same as was found in the as-quenched specimens. Figure 9 reveals the shallow-dimpled rupture appearance of the fast fracture area, characteristic of the high fracture toughness.[17] This, too, was similar to the appearance of the fracture surface of the as-quenched specimens.

Microstructure and Fatigue Crack Growth Rates After Tempering at 300°C

Tempering at 300°C led to a significant drop in yield strength, as well as to a drop in fracture toughness, as shown in Figs. 1(a) and 1(b). Transmission electron microscopy revealed that substantial growth of lath boundary precipitates had occurred, as shown in Fig. 10.[12] In the fast fracture area, the lath boundary precipitation led to a change in appearance from dimpled rupture, characteristic of the 225°C tempered specimen, to quasi-cleavage. In Fig. 11, a scanning electron micrograph

of a surface in the fast fracture region, quasi-cleavage fracture features are evident. The fatigue crack growth rates did not reflect the lowering of properties that were found in the fracture toughness tests. In fact, the parameters from the Paris relation derived from crack growth data show a slight improvement in fatigue properties. The fatigue fracture surface appearance was unchanged, as shown in Fig. 12 where ΔK was 35 ksi-in.$^{1/2}$ (38 MN/m$^{3/2}$) and the coefficient, m, remained approximately 2. There was no increase in growth rates even when maximum stress intensity, K_{max}, approached K_{IC}.

The deterioration of fracture toughness in the 260-315°C tempering range was a result of "tempered martensite embrittlement", which is a common characteristic of quenched and tempered steels.[18] In this steel, the embrittling effect was attributed to the presence of additional precipitates at martensite lath boundaries,[12] leading to a decrease in fracture toughness,[19] characterized by the quasi-cleavage fracture. Lath boundary precipitation has also been observed in other steels after tempering in this temperature range.[20,21]

The structural features causing tempered martensite embrittlement did not affect fatigue crack propagation rates significantly in this steel. A similar discrepancy between toughness and crack growth rates was observed in 4340 steel by Anctil and Kula.[11] Because the fatigue crack growth properties are not deleteriously affected by the presence of lath boundary precipitates, it can be concluded that some of the microstructural features controlling fracture toughness do not affect fatigue crack propagation substantially. Plastic

deformation of the matrix is a requisite feature of fatigue crack growth, and for a given set of test conditions, the characteristics of the matrix largely govern the crack growth rates.

The influence of brittle particles on crack growth rates is unclear; there is conflicting evidence on the role of such particles.[22-24] Pelloux[23] found increased growth rates in aluminum alloys with increased volume fraction of particles, but in his experiments the changes in volume fraction were large. Glassman and McEvily[24] found decreased rates in aluminum alloys with an increase in particle volume fraction. This work, however, was carried out at very high stresses with thin sheets under conditions of plane stress.

Static fracture does not necessarily require plastic deformation; failure may be by cleavage. Fracture under static loading is highly sensitive to microstructural features, especially those offering easy crack paths. Thus, it is not surprising that certain heat treating procedures may cause a severe drop in fracture toughness without appreciably changing fatigue crack growth behavior.

Microstructure and Fatigue Crack Growth After Tempering at 500°C

Tempering at 500°C led to a small increase in yield strength, as shown in Fig. 1(a). This increase was caused by secondary hardening. There was a concomitant drop in fracture toughness, as shown in Fig. 1(b). Transmission electron microscopy revealed Fe_3C precipitate networks at lath boundaries.[12] Although no molybdenum carbides were detected, they were undoubtedly present in small quantities accounting for the rise in strength. The 600°C tempering treatment (discussed in detail later) produced substantial amounts of easily identified molybdenum carbide.

The fatigue crack growth rate increased considerably on tempering at 500°C, as compared with the 300°C tempered specimens. The exponent, m, was 2.55. Figure 13 shows the appearance of the fatigue region at ΔK of 31 ksi-in.$^{1/2}$ (34 MN/m$^{3/2}$). The corresponding crack growth rate was 2.5×10^{-5} in./cycle (6.3×10^{-4} mm/cycle). The composite photograph reveals that the fatigue surface contained features similar to those observed in the 300°C tempered condition. It was concluded that the thickened and extensive cementite films, as well as alloy carbides, led to the observed increase in growth rates for the 500°C tempered specimen. With extensive films present, the average crack growth rates reflected the lower toughness of the steel in this condition.

Microstructure and Fatigue Crack Growth After Tempering at 600°C

A large increase in yield strength and a further decrease in fracture toughness were observed for specimens tempered at 600°C. The results are shown in Figs. 1(a) and 1(b). Transmission electron microscopy revealed Mo_2C dispersed within the martensite laths; electron diffraction showed that Fe_3C was no longer present in specimens tempered at this temperature.[12] Extensive precipitation was revealed by optical metallography, as shown in Fig. 14. The fast fracture region contained large regions of integranular failure along with quasi-cleavage features.

The fatigue crack growth rates increased significantly over those characteristic of specimens tempered at lower temperatures. As K_{max} approached K_{IC} the growth rates increased to very high values, as shown in Fig. 2(e). The exponent, m, increased to 4.5, and there was considerable scatter in the growth rate data. Scanning electron microscopy of the fatigue surface revealed the significant reasons for the increased crack

growth rate and the cause of the larger scatter in the data. Figure 15 is a composite photograph of the fatigue surface taken from a specimen which exhibited a crack growth rate of 1×10^{-5} in./cycle (2.5×10^{-4} mm/cycle) at ΔK of 21.5 ksi $in.^{1/2}$ (23.5 $MN/m^{3/2}$). The figure shows that an intergranular failure mode was present in the fatigue region, as well as the usual ductile mode characteristic of a fatigue fracture. The added mode was observed at both low and high level of K_{max} with respect to the low K_{IC} produced by this heat treatment. The increase in growth rates and the large scatter for the 600°C tempered specimen can be attributed to the added intergranular mode of failure present during fatigue in the specimen tempered at 600°C. Similar observations have been made on other steels.[6] Ritchie and Knott[25] saw the presence of grain boundary cracking during fatigue in "temper brittle" EN30A (embrittled at 540°C) under plane strain conditions. They also found an increase in the exponent describing the fatigue crack growth properties. Rayner et al.[26] found that in similar steel, Mo_2C nucleated at cementite/ferrite interfaces as well as on matrix dislocations and at grain boundaries. This precipitation would lead to extensive lath boundary and grain boundary precipitation of the new carbide. Small precipitates would also pin dislocations accounting for the increased strength. With matrix dislocations unable to move, cracking at grain boundaries could occur during cyclic loading. Carbide films at prior austenite grain boundaries have been shown to lead to deterioration in properties.[27] However, a degradation in fracture strength has also been attributed to impurity segregation to these boundaries.[28] The only clear result was that the tempering treatment producing peak secondary hardening led to increased fatigue crack growth rates.

Microstructural Environmental Interaction and Fatigue Crack Propagation on the 5Mo-0.3C Steel

Having established that in air the fatigue crack growth rates vary with microstructure, it was necessary to evaluate the effect of environmental-microstructural interaction. Limited fatigue tests in a dry argon environment were carried out to do this.

Figures 3(a) and (b) show the fatigue crack growth rates in dry argon for the as-quenched and 600°C tempering treatments, respectively. The broken lines represent the ambient properties. It is clear that moist air environments enhance crack growth rates in the as-quenched steel. This has been repeatedly shown on similar high strength steels.[8,29] The 600°C tempered material showed less sensitivity to environment, however. The fatigue fracture surface for the specimen tested in dry argon still showed evidence of intergranular failure modes both in low and high ΔK regions. For this microstructure, having unusually poor fracture toughness, the undesirable features dominated environmental effects.

SUMMARY AND CONCLUSIONS

The fatigue crack growth properties and fracture toughness properties for the 5Mo-0.3C steel are compared for the different tempering treatments in Fig. 16 (the crack growth properties are shown as the number of cycles to grow 1 in., 25.4 mm, at a given ΔK). This figure shows that after tempering treatments through 300°C, fatigue crack growth properties are insensitive to the microstructural changes that clearly affect fracture toughness properties. Figure 16 also shows that tempering at 500°C and 600°C, however, lead to changes that adversely affect both fracture toughness and fatigue crack growth properties.

The general conclusions gleened from the study of fatigue crack propagation in 5Mo-0.3C steel are summarized below:

(1) In this steel, fracture toughness properties were more sensitive to microstructural change than were fatigue crack growth rates. In particular, tempering at 300°C led to a substantial decrease in fracture toughness while it had little effect on fatigue crack growth rates.

(2) The secondary hardening process, however, can adversely affect both fatigue crack growth and fracture toughness properties. In particular, tempering at both 500°C and 600°C in this steel led to microstructures having increased crack growth rates under cyclic loading at K_{max} values well below K_{IC}.

(3) The presence of additional failure modes in the fatigue area, such as intergranular fracture, causes an increase in crack growth rates. These changes are reflected in the values of the empirical constants from the Paris relation.

(4) Limited testing in a dry argon environment showed variation in sensitivity to moisture effects during crack propagation with microstructure. In particular, the as-quenched material exhibited rates at least 50% higher in moist air as in argon, while for the 600°C tempered specimen the data for the two environments overlapped.

(5) The general fatigue crack growth properties in the as-quenched 5Mo-0.3C steel, which had an autotempered martensite structure, were comparable to other high strength steels in an ambient environment. The crack growth rates followed an approximate second power dependence.

ACKNOWLEDGEMENTS

The author wishes to express his deep appreciation to Professors V. F. Zackay and E. R. Parker for their constant encouragement and guidance during the course of this investigation.

This research was performed partially under the auspices of the U. S. Atomic Energy Commission through the Inorganic Materials Research Division of the Lawrence Berkeley Laboratory, and partially under the auspices of the Army Materials and Mechanics Research Center, Watertown, Massachusetts.

REFERENCES

1. P. Paris and F. Erdogan: Trans. ASME, 1963, vol. 85, pp. 528-534.
2. H. H. Johnson and P. C. Paris: Eng. Fract. Mech., 1968, vol. 1, pp. 3-45.
3. G. R. Chanani, S. D. Antolovich, and W. W. Gerberich: Met. Trans. 1972, vol. 3, pp. 2661-2672.
4. W. G. Clark, Jr.: Eng. Fract. Mech., 1968, vol. 1, pp. 385-398.
5. N. E. Frost, L. P. Pook, and K. Denton: Eng. Fract. Mech., 1971, vol. 3, pp. 109-126.
6. C. E. Richards and T. C. Lindley: Eng. Fract. Mech., 1972, vol. 4, pp. 951-978.
7. P. R. Evans, N. B. Owens, and B. E. Hopkins: Eng. Fract. Mech., 1971, vol. 3, pp. 463-473.
8. R. P. Wei, P. M. Talda, and C. Li: Fatigue Crack Propagation, ASTM, STP 415, pp. 460-480, ASTM, Philadelphia, PA, 1967.
9. F. A. Hieser and W. Mortimer: Met. Trans., 1972, vol. 3, p. 2119-2123.
10. G. A. Miller: Trans. ASM, 1968, vol. 61, pp. 442-448.
11. A. A. Anctil and E. B. Kula: Effects of Environment and Complex Load History and Fatigue Life, ASTM, STP 462, pp. 297-317, ASTM Philadelphia, PA, 1970.
12. R. D. Goolsby: Ph. D. Thesis, University of California, Berkeley, LBL-405, Nov. 1971.
13. 1973 Annual Book of ASTM Standards, part 31 (American Society for Testing and Materials, PA, 1973), p. 960.
14. J. Mandel: The Statistical Analysis of Experimental Data, pp. 247-250, Wiley-Interscience, New York, 1964.

15. P. M. Kelly and J. Nutting: J. Iron Steel Inst., 1961, vol. 197, pp. 199-211.

16. J. F. Throop and G. A. Miller: Achievement of High Fatigue Resistance in Metals and Alloys, ASTM STP 467, pp. 154-168, ASTM, Philadelphia, PA, 1970.

17. C. D. Beachem and R. M. N. Pelloux: Fracture Toughness Testing and Its Applications, ASTM STP 381, pp. 210-245, ASTM, Philadelphia, PA, 1965.

18. E. B. Kula and A. A. Anctil: J. Mater., 1969, vol. 4, pp. 817-841.

19. T. B. Cox and J. R. Low, Jr.: Met. Trans., 1974, vol. 5, pp. 1457-1470.

20. B. S. Lement, B. L. Averbach and M. Cohen: Trans. ASM, 1954, vol. 46, pp. 851-881.

21. Y. H. Liu: Trans. ASM, 1969, vol. 62, pp. 55-63.

22. C. Laird: Fatigue Crack Propagation ASTM, STP 415, pp. 131-180, ASTM, Philadelphia, PA, 1967.

23. R. M. N. Pelloux: Trans. ASM, 1964, vol. 57, p. 511-518.

24. L. H. Glassman and A. J. McEvily, Jr.: NASA TN D-928, 1962.

25. R. O. Ritchie and J. F. Knott: Acta Met., 1973, vol. 21, pp. 639-648.

26. D. Raynor, J. A. Whiteman, and R. W. K. Honeycombe: J. Iron Steel Inst., 1966, vol. 204, pp. 349-354.

27. J. R. Low, Jr.: Trans. TMS-AIME, 1969, vol. 245, pp. 2481-2494.

28. J. Plateau, G. Henry and C. Crussard: Rev. Metall., 1957, vol. 54, pp. 200-216.

29. E. P. Dahlberg: Trans. ASM, 1965, vol. 58, pp. 46-53.

Table I. Chemical analyses of alloys used.

Alloy No.	Mo	Mn	C	Fe
723-15	5.0	0.66	0.28	balance
723-16	5.1	0.70	0.26	balance
723-17	5.1	0.66	0.26	balance
723-18	5.2	0.62	0.28	balance

FIGURE CAPTIONS

Fig. 1. (a) Yield strength as a function of tempering temperature.

(b) Plane strain fracture toughness as a function of tempering temperature.

Fig. 2. (a) Fatigue crack propagation rate vs stress intensity range for the as-quenched 5Mo-0.3C steel. Data from specimens 15-1 and 18-1.

(b) Fatigue crack propagation rate vs stress intensity range for the 225°C tempered steel. Data from specimens 16-2 and 18-2.

(c) Fatigue crack propagation rates vs stress intensity range for the 300°C tempered steel. Data from specimens 15-3 and 16-3.

(d) Fatigue crack propagation rates vs stress intensity range for the 500°C tempered steel. Data from specimens 15-4 and 18-4.

(e) Fatigue crack propagation rates vs stress intensity range for the 600°C tempered steel. Data from specimen 15-5.

Fig. 3. (a) Fatigue crack propagation rates vs stress intensity range for the as-quenched 5Mo-0.3C steel carried out in dry argon. Data from specimen 17-1. Dashed line represents rates in air.

(b) Fatigue crack propagation vs stress intensity range for the 600°C tempered steel carried out in dry argon. Data from specimen 17-5. Dashed line represents rates for steel in same condition in air.

Fig. 4. Microstructure of the as-quenched material.

Fig. 5. Structure of as-quenched specimen showing in bright field (a) autotempered, dislocated martensite laths, and in dark field (b) cementite precipitation.

Fig. 6. Fatigue fracture region in as-quenched material. ΔK-35 ksi-in.$^{1/2}$ (38-MN/m$^{3/2}$). Composite enlargement shows quasi-cleavage at A, fatigue cracking through bulk microstructure at B, and local striations at C.

Fig. 7. Fatigue fracture showing striations in as-quenched material. K = 40 ksi-in.$^{1/2}$ (43.5 MN/m$^{3/2}$).

Fig. 8. Comparisons of fatigue crack propagation rate vs stress intensity range of as-quenched steel with rates reported for other high-strength steels (A-Ref. 9, B-Rev. 11, C-Ref. 16 and D-Ref. 7).

Fig. 9. Fast fracture appearance of 225°C tempered steel showing primarily dimpled rupture characteristics.

Fig. 10. Structure of 300°C tempered material showing in bright field (a) cementite precipitation in lath boundaries and dark field (b) of cementite reflection.

Fig. 11. Fast fracture appearance of 300°C tempered steel showing quasi-cleavage characteristics.

Fig. 12. Composite of fatigue fracture surface of 300°C tempered steel. General fatigue appearance resembles that of as-quenched material. ΔK = 35 ksi-in.$^{1/2}$ (38 MN/m$^{3/2}$).

Fig. 13. Composite SEM fractograph showing fatigue fracture surface of 500°C tempered steel. Quasi-cleavage visible. ΔK - 31 ksi-in.$^{1/2}$ (34 MN/m$^{3/2}$).

Fig. 14. Microstructure of 600° tempered steel.

Fig. 15. Composite SEM fractograph showing fatigue fracture surface of 600°C tempered steel. Intergranular mode of failure evident in fatigue area. ΔK = 21 ksi-in.$^{1/2}$ (23 MN/m$^{3/2}$).

Fig. 16. Comparison of fatigue crack growth and fracture toughness. Properties of the different tempering treatments given the 5Mo-0.3C steel. Number of cycles to grow one inch at a constant stress intensity range are used to measure crack growth characteristics.

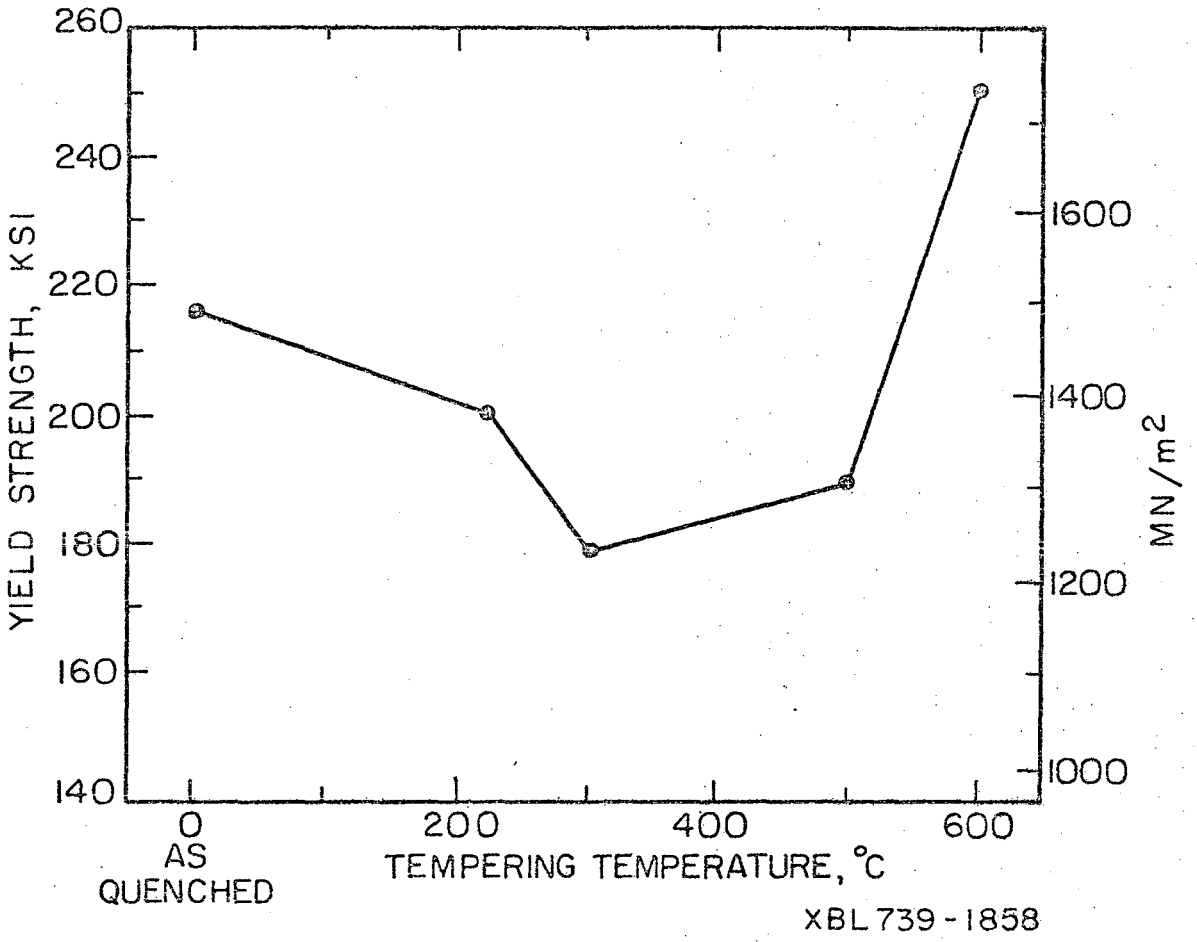
260
240
220
200
180
160
140
YIELD STRENGTH, KSI
1600
1400
1200
1000
MN/m2
0
AS
QUENCHED
200
400
600
TEMPERING TEMPERATURE, °C
XBL 739-1858

Fig. 1a

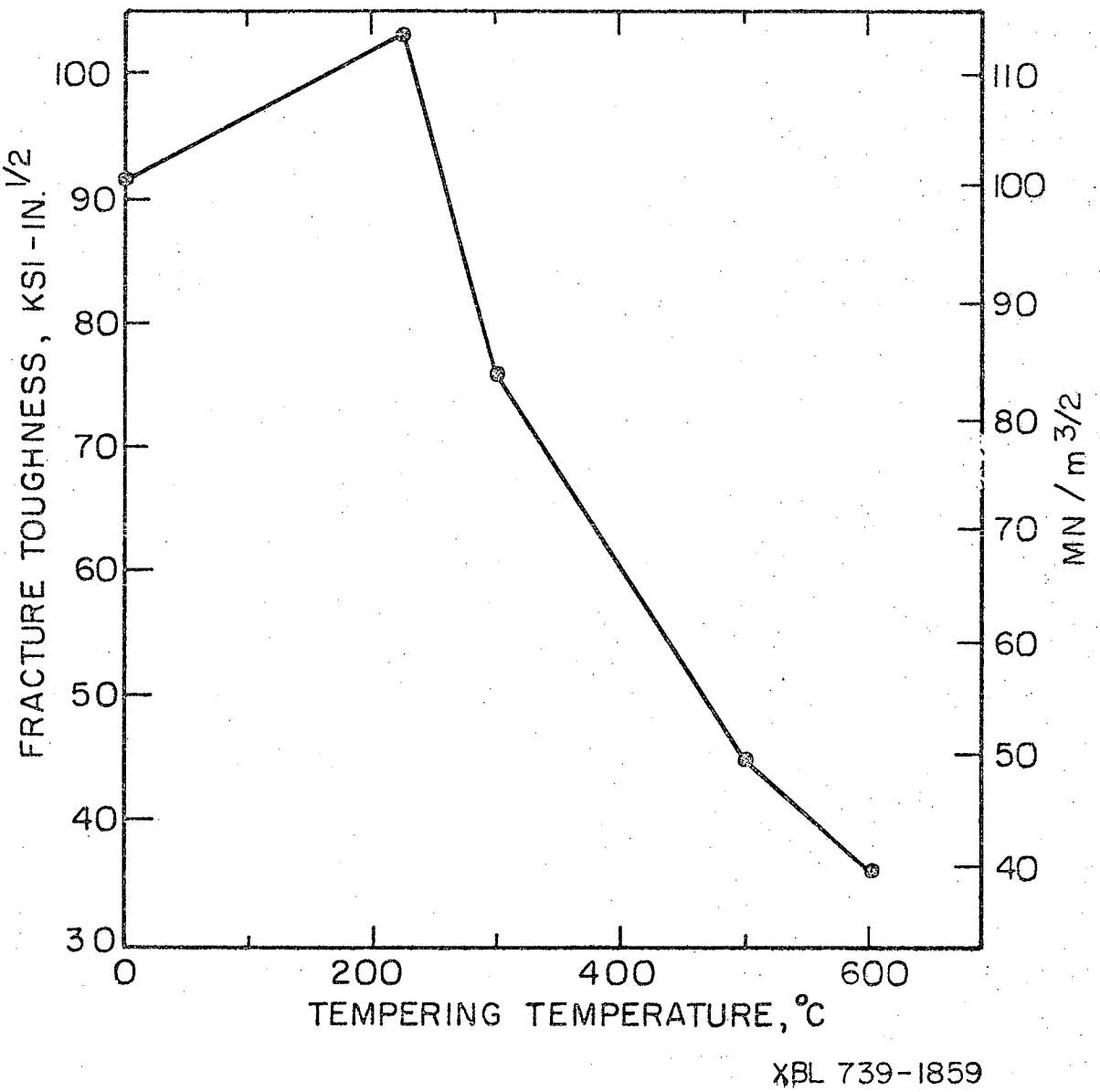
FRACTURE TOUGHNESS, KSI-IN.$^{1/2}$
MN / m$^{3/2}$
TEMPERING TEMPERATURE, °C
100
90
80
70
60
50
40
30
110
100
90
80
70
60
50
40
0
200
400
600
XBL 739-1859

Fig. 1b

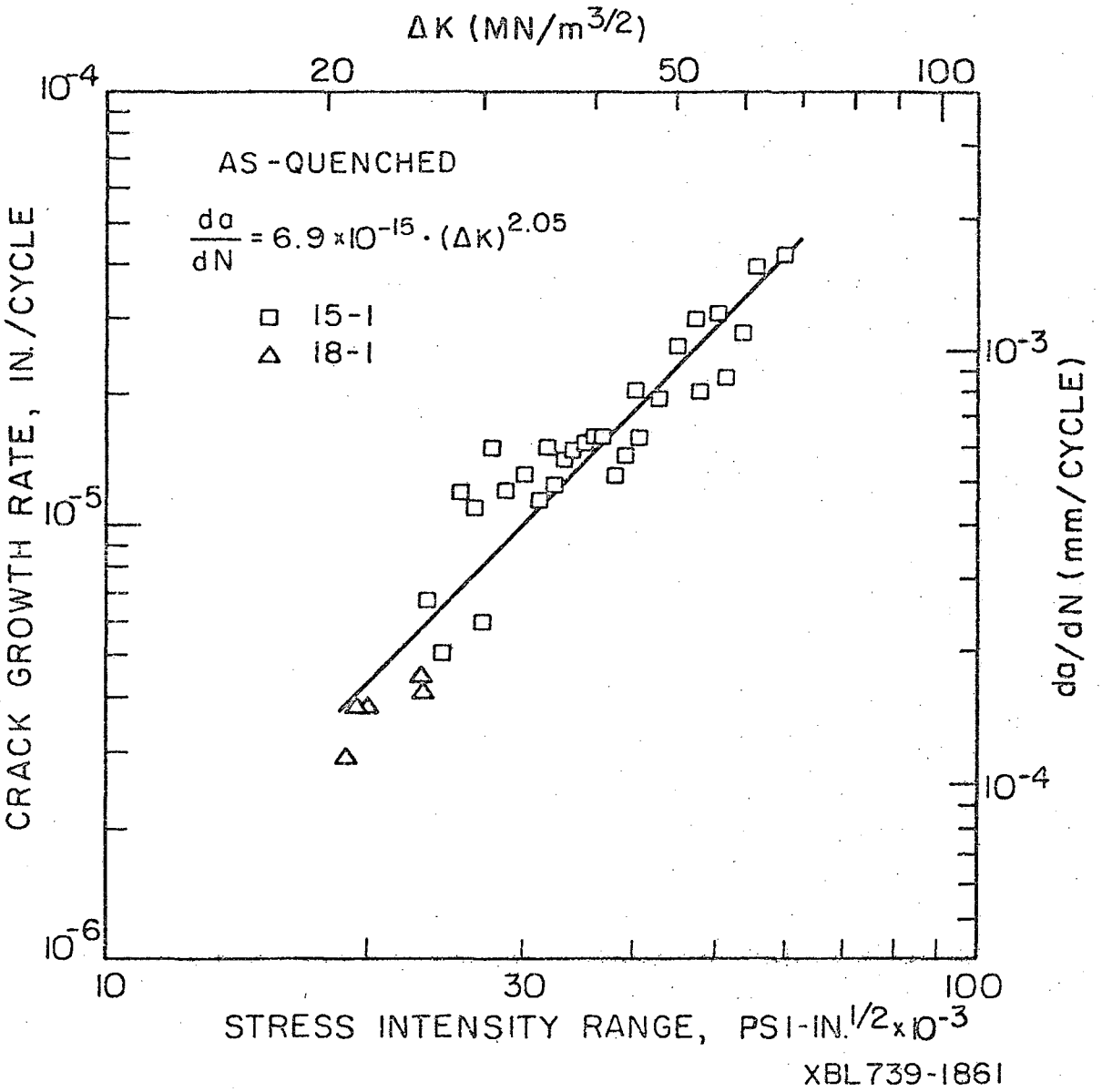
ΔK (MN/m3/2)
20
50
100
AS-QUENCHED
da/dN = 6.9 x 10-15 · (ΔK)2.05
15-1
18-1
CRACK GROWTH RATE, IN./CYCLE
da/dN (mm/CYCLE)
10-4
10-5
10-6
10-3
10-4
10
30
100
STRESS INTENSITY RANGE, PSI-IN.1/2 x 10-3
XBL739-1861

Fig. 2a

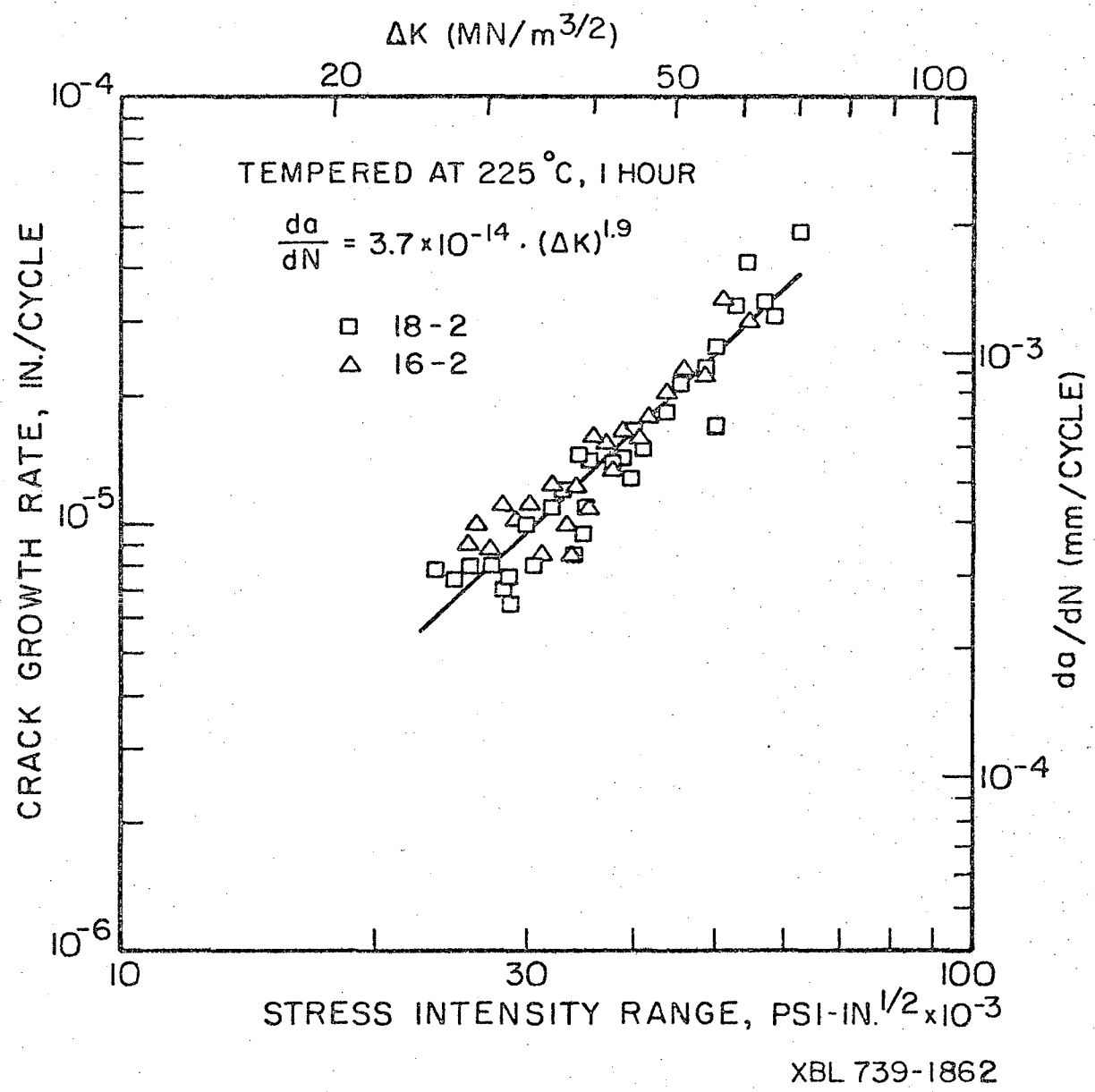
ΔK (MN/m^3/2)
20
50
100
TEMPERED AT 225 °C, 1 HOUR
da/dN = 3.7 x 10^-14 . (ΔK)^1.9
18-2
16-2
CRACK GROWTH RATE, IN./CYCLE
10^-4
10^-5
10^-6
10^-3
10^-4
da/dN (mm/CYCLE)
10
30
100
STRESS INTENSITY RANGE, PSI-IN.^1/2 x 10^-3
XBL 739-1862

Fig. 2b

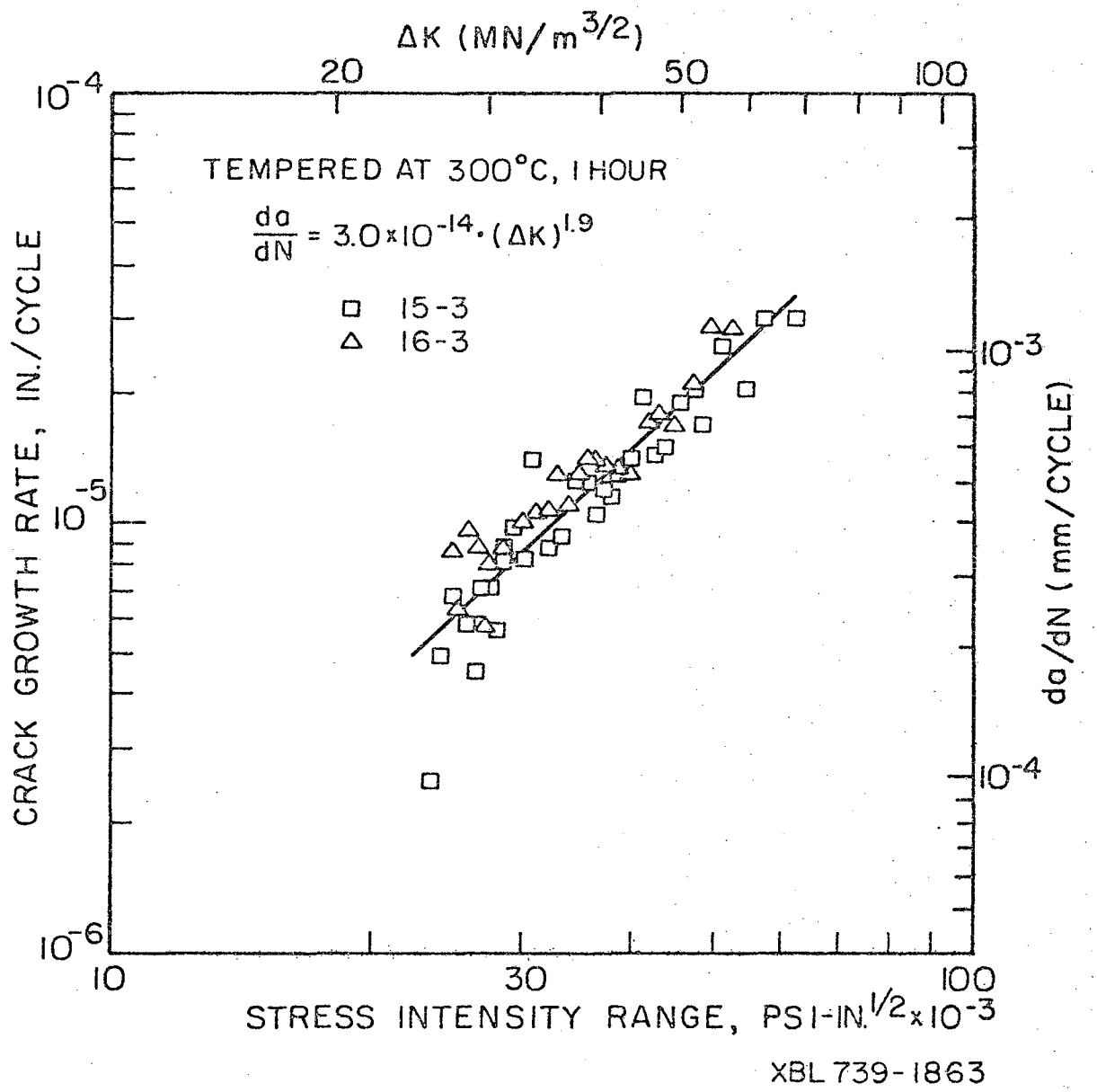
ΔK (MN/m^3/2)
20
50
100
TEMPERED AT 300°C, 1 HOUR
da/dN = 3.0×10^-14 · (ΔK)^1.9
15-3
16-3
CRACK GROWTH RATE, IN./CYCLE
10^-4
10^-5
10^-6
10^-3
10^-4
da/dN (mm/CYCLE)
10
30
100
STRESS INTENSITY RANGE, PSI-IN.^1/2 x 10^-3
XBL 739-1863

Fig. 2c

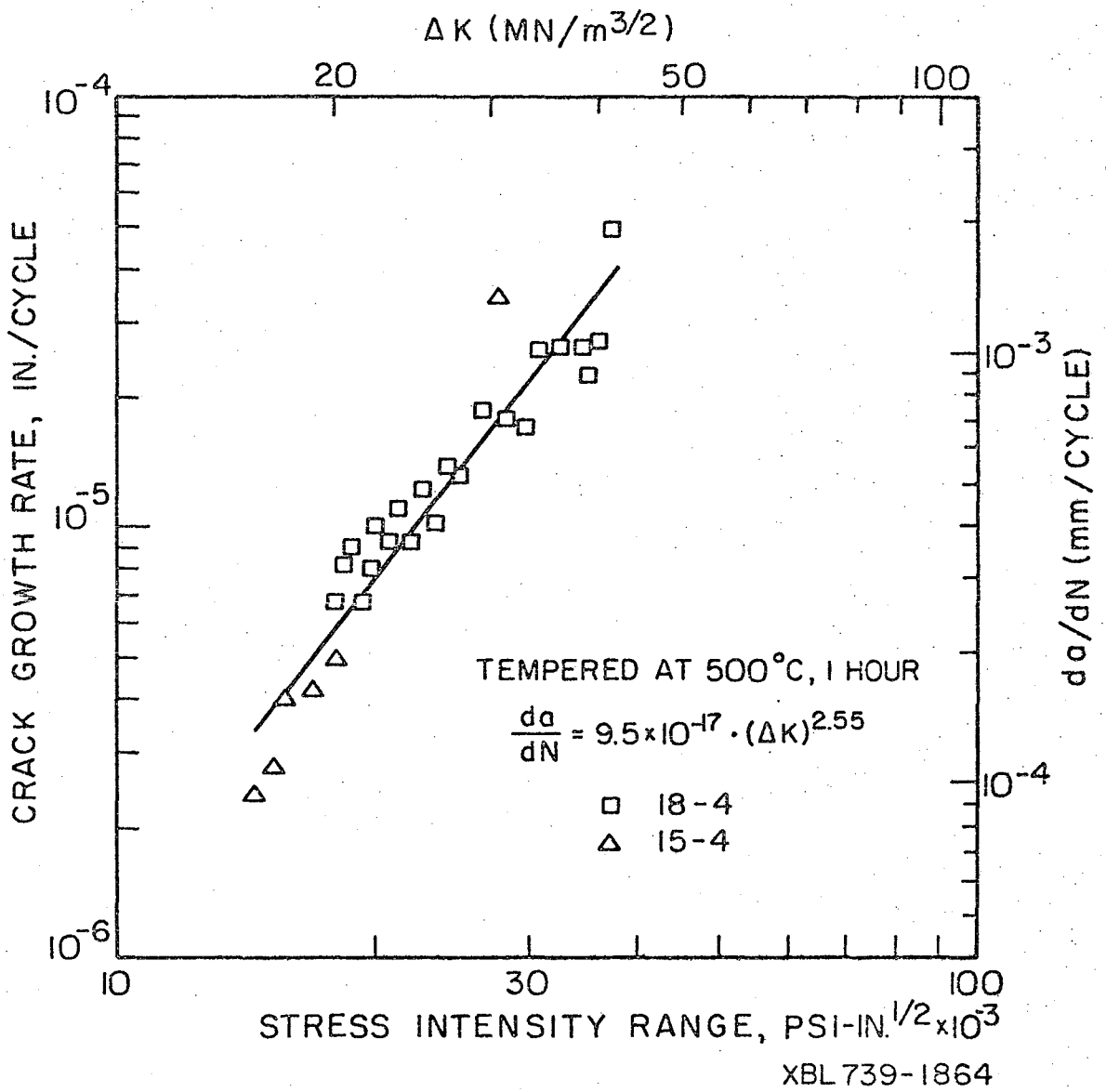
ΔK (MN/m3/2)
20
50
100
10-4
10-5
10-6
CRACK GROWTH RATE, IN./CYCLE
10-3
10-4
da/dN (mm/CYCLE)
TEMPERED AT 500°C, 1 HOUR
da/dN = 9.5x10-17 · (ΔK)2.55
18-4
15-4
10
30
100
STRESS INTENSITY RANGE, PSI-IN.1/2x10-3
XBL 739-1864

Fig. 2d

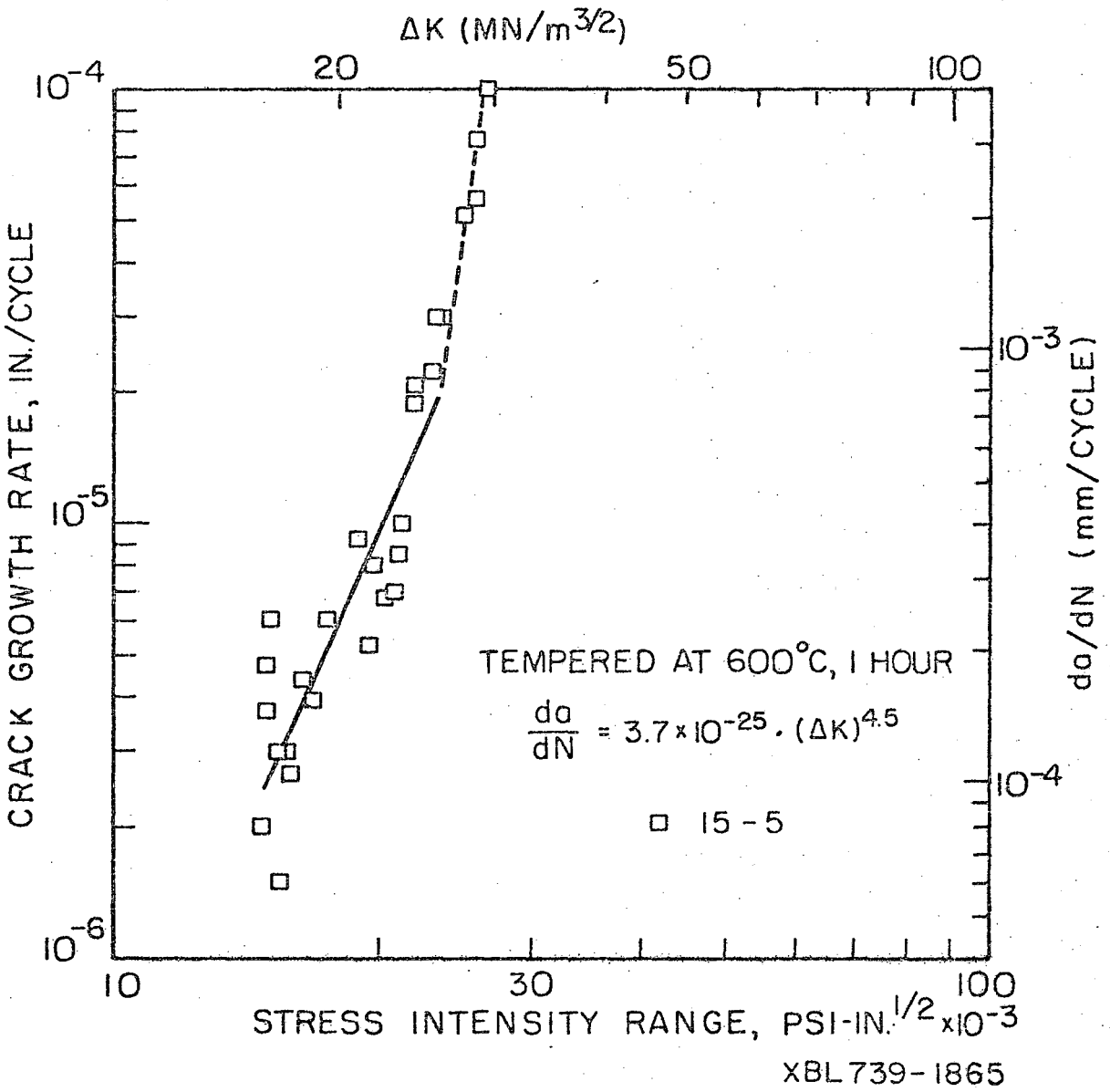
ΔK (MN/m^3/2)
20
50
100
10^-4
10^-5
10^-6
CRACK GROWTH RATE, IN./CYCLE
10^-3
10^-4
da/dN (mm/CYCLE)
TEMPERED AT 600°C, 1 HOUR
da/dN = 3.7 x 10^-25 . (ΔK)^4.5
15 - 5
10
30
100
STRESS INTENSITY RANGE, PSI-IN.^1/2 x10^-3
XBL739-1865

Fig. 2e

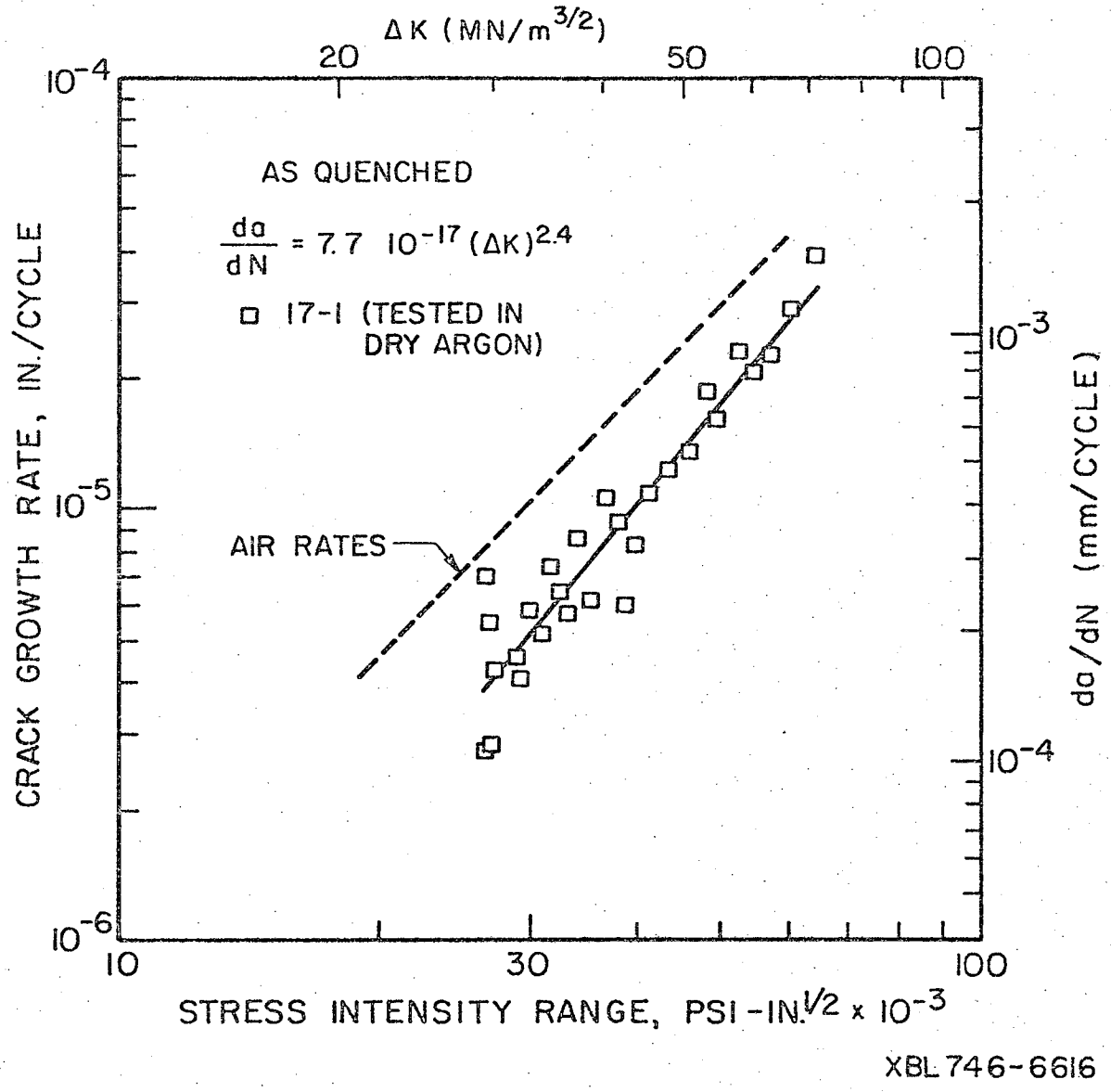
ΔK (MN/m^3/2)
20
50
100
AS QUENCHED
da/dN = 7.7 10^-17 (ΔK)^2.4
17-I (TESTED IN DRY ARGON)
AIR RATES
CRACK GROWTH RATE, IN./CYCLE
da/dN (mm/CYCLE)
10^-4
10^-5
10^-6
10^-3
10^-4
10
30
100
STRESS INTENSITY RANGE, PSI-IN.^1/2 x 10^-3
XBL 746-6616

Fig. 3a

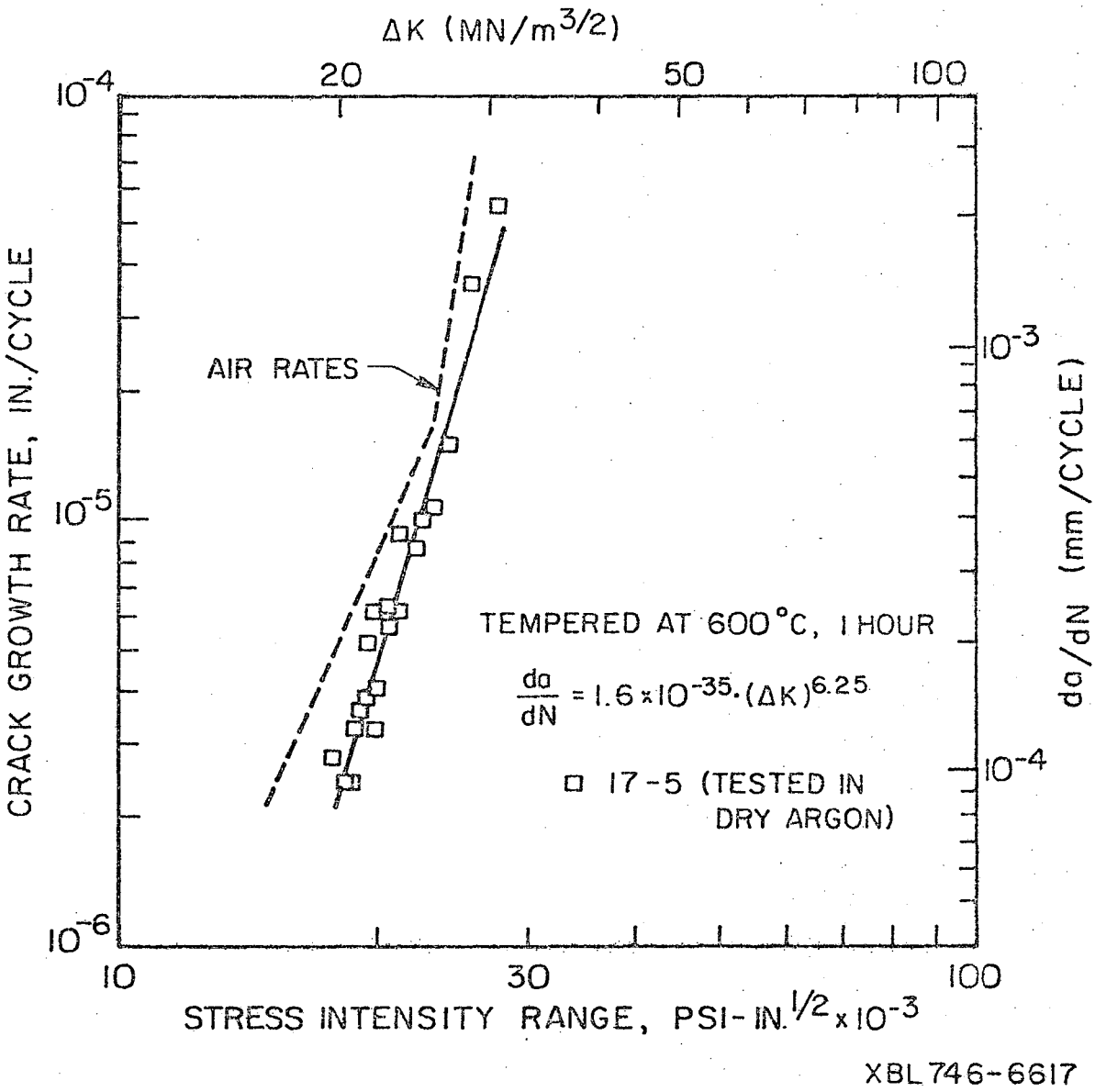
ΔK (MN/m3/2)
20
50
100
10-4
10-5
10-6
CRACK GROWTH RATE, IN./CYCLE
AIR RATES
TEMPERED AT 600°C, 1 HOUR
da/dN = 1.6 x 10-35. (ΔK)6.25
17-5 (TESTED IN DRY ARGON)
10-3
10-4
da/dN (mm/CYCLE)
10
30
100
STRESS INTENSITY RANGE, PSI-IN.1/2 x 10-3
XBL746-6617

Fig. 3b

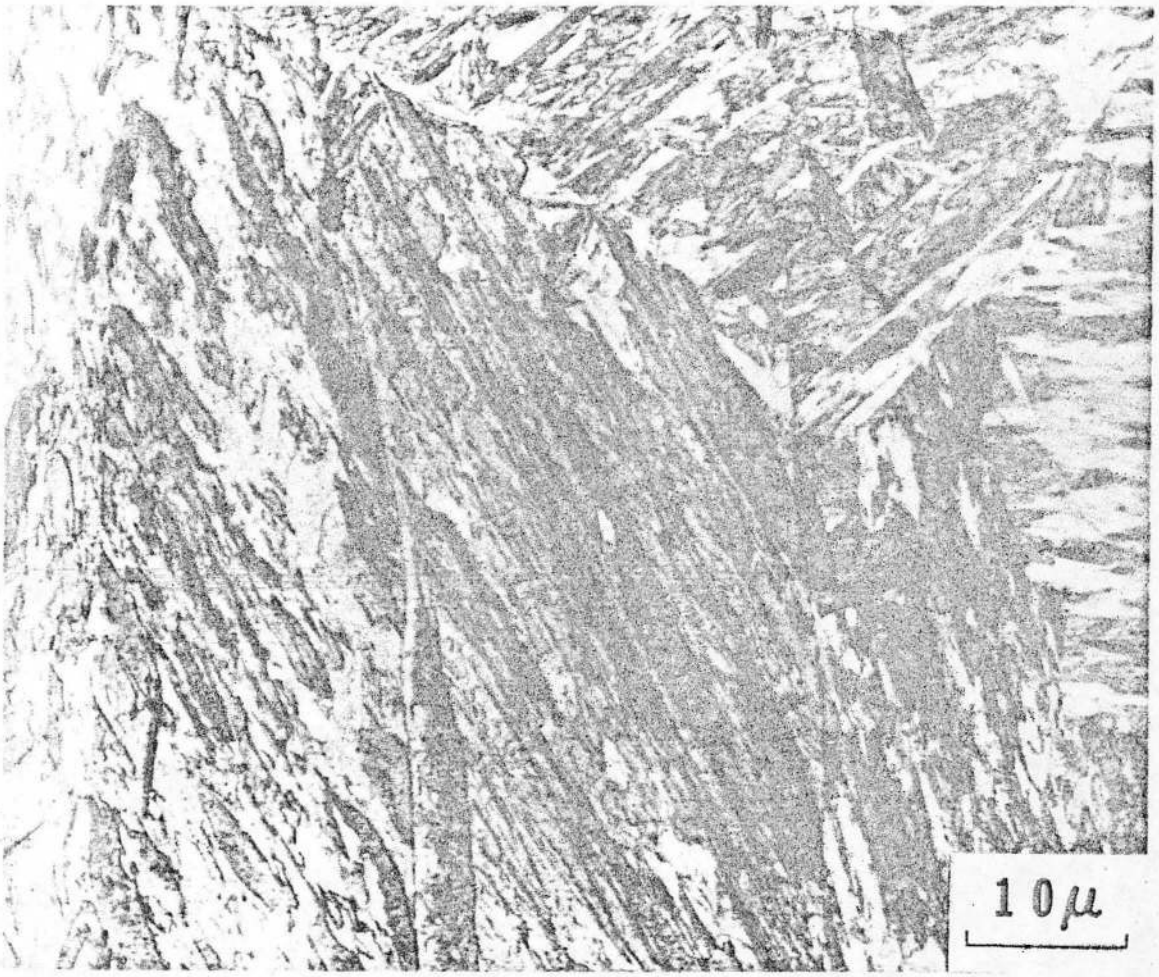

XBB 739-5584

Fig. 4

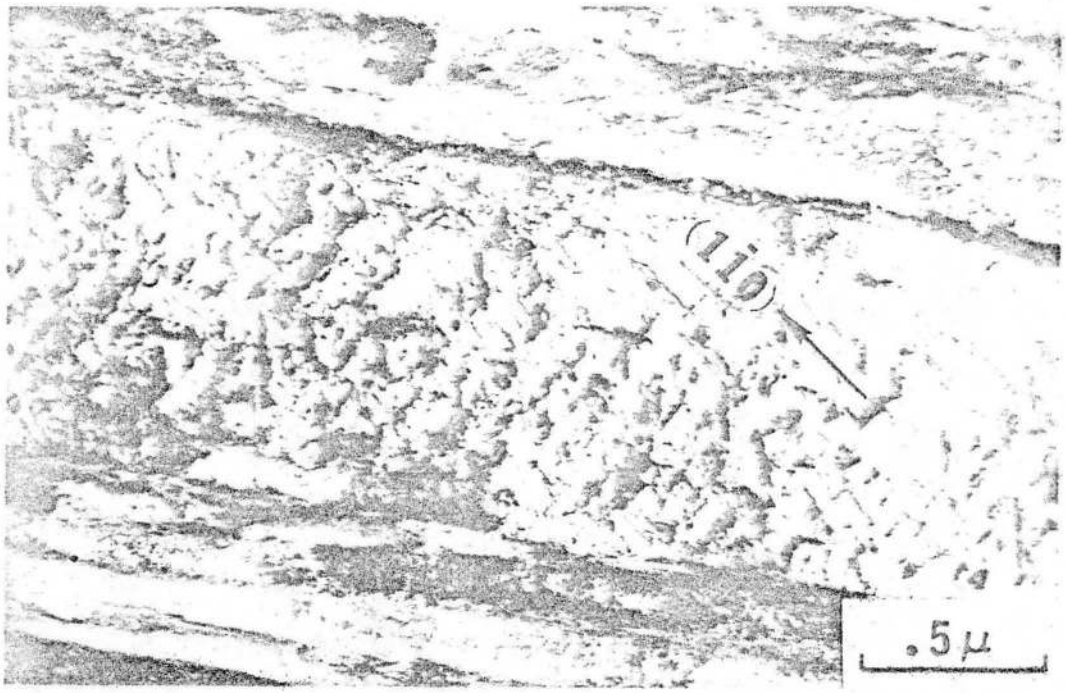

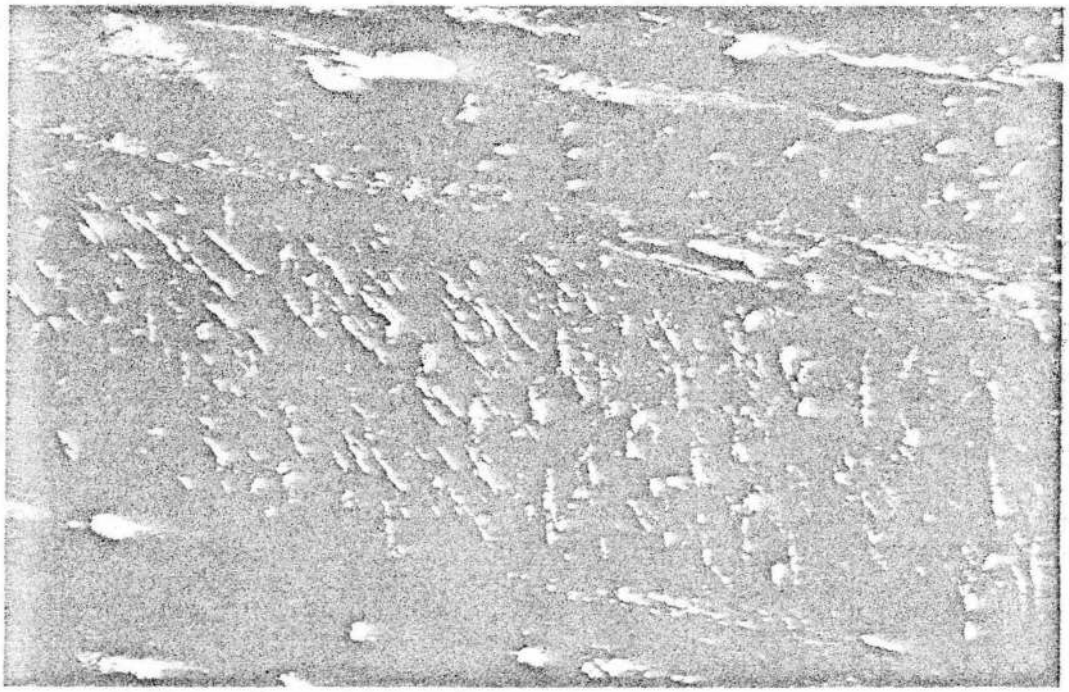

XBB 7111-5567

Fig. 5

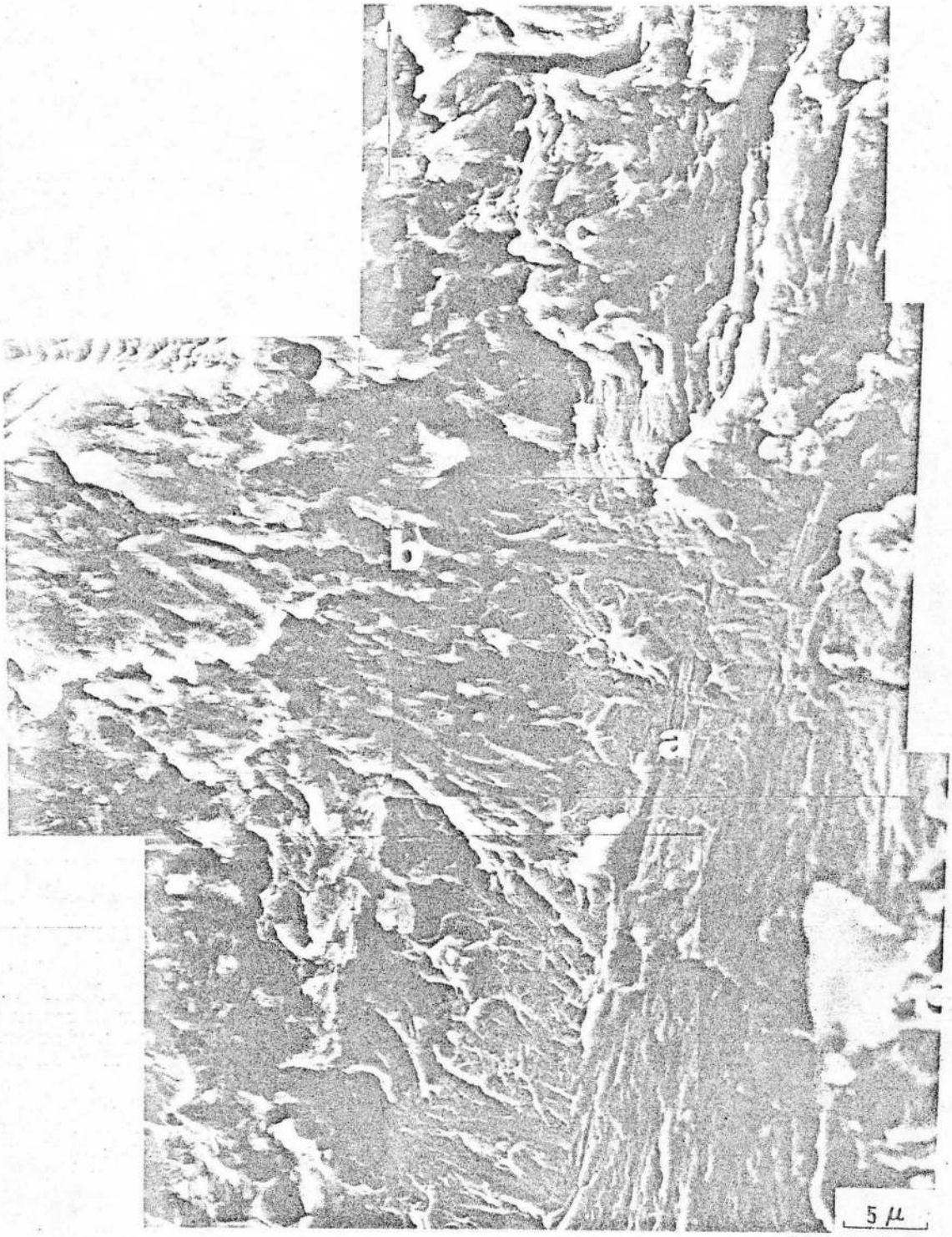

XBB 749-6331

Fig. 6

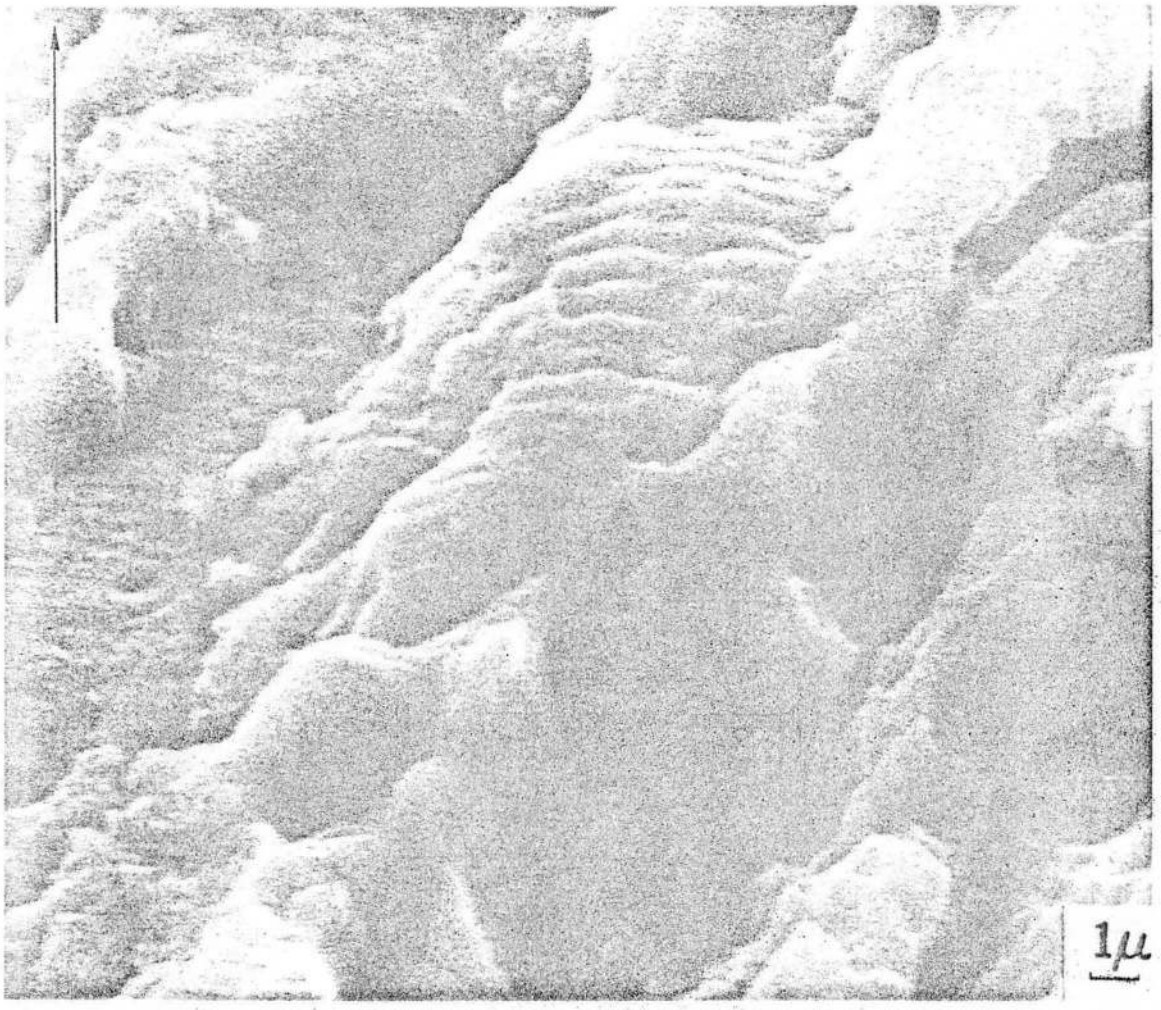

XBB 749-6332

Fig. 7

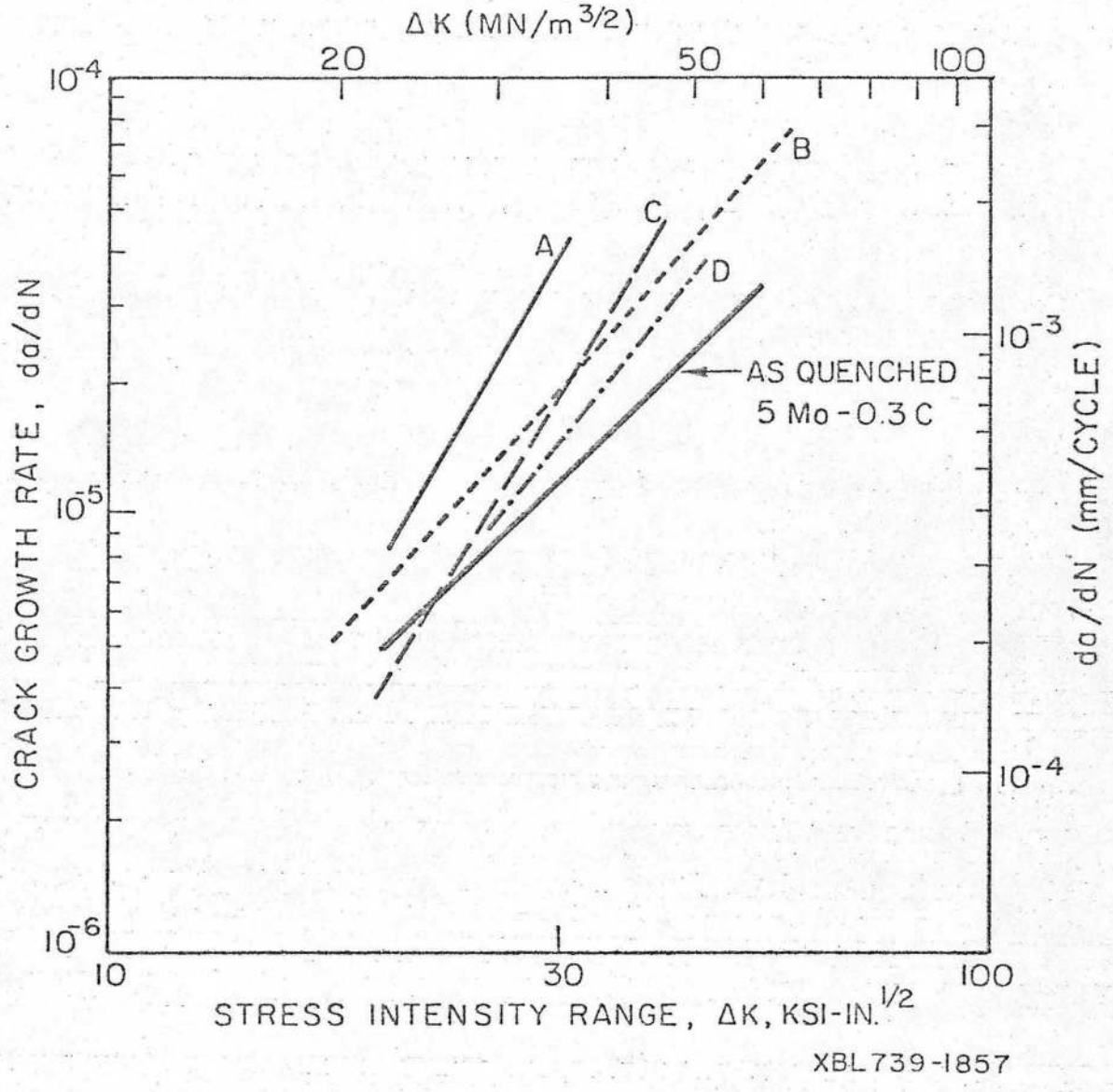
ΔK (MN/m^3/2)
20
50
100
10^-4
10^-5
10^-6
10^-3
10^-4
A
B
C
D
AS QUENCHED
5 Mo - 0.3 C
CRACK GROWTH RATE, da/dN
da/dN (mm/CYCLE)
10
30
100
STRESS INTENSITY RANGE, ΔK, KSI-IN.^1/2
XBL739-1857

Fig. 8

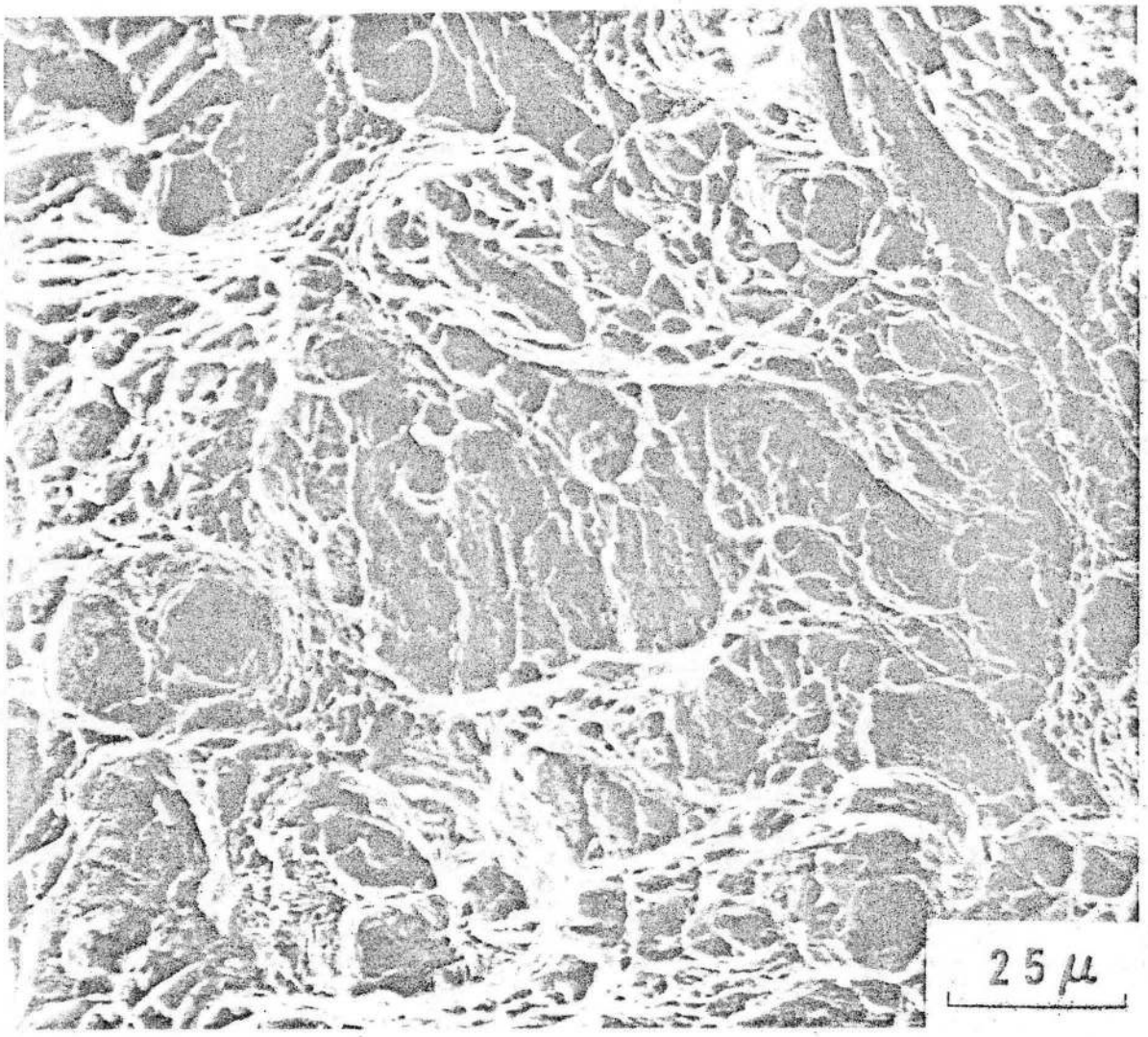

XBB 739-5587

Fig. 9

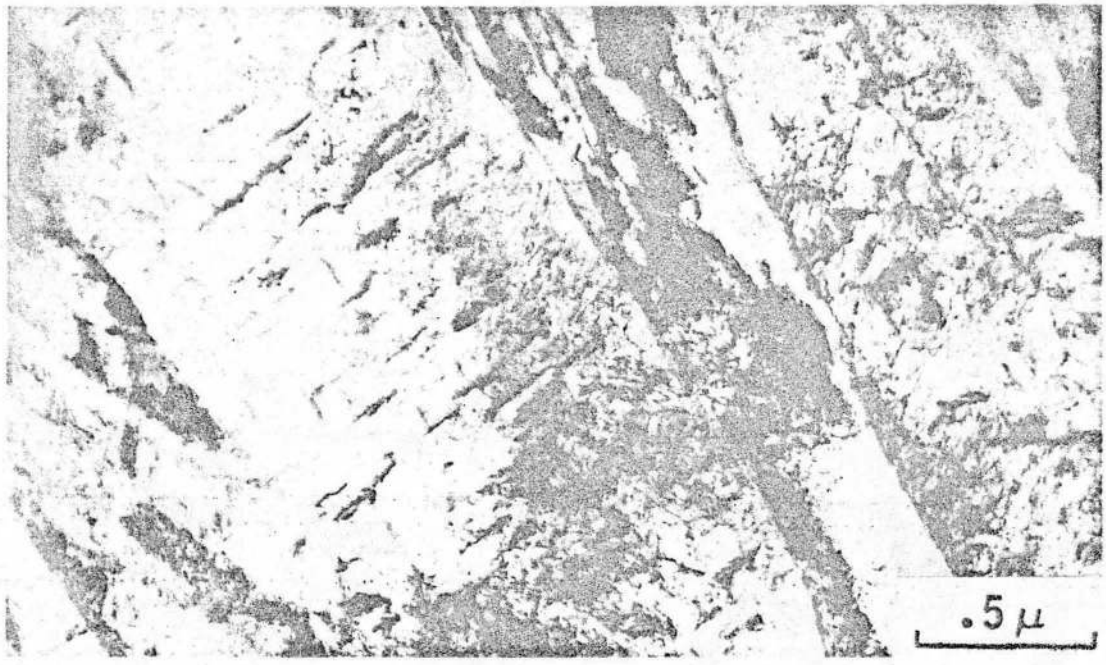

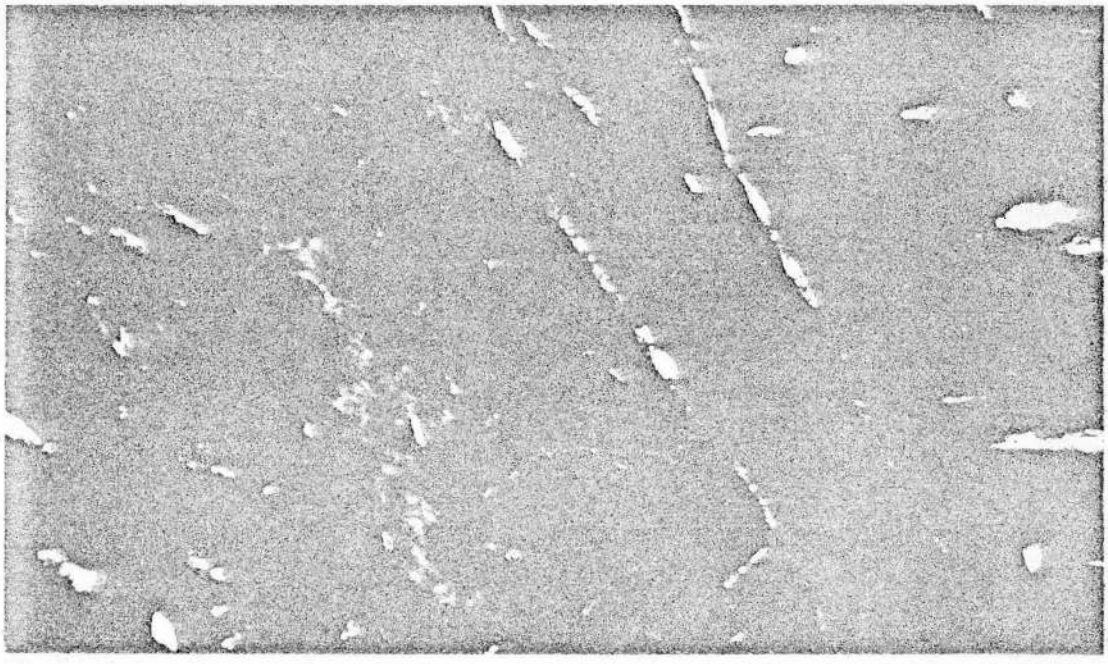

XBB 7111-5568

Fig. 10

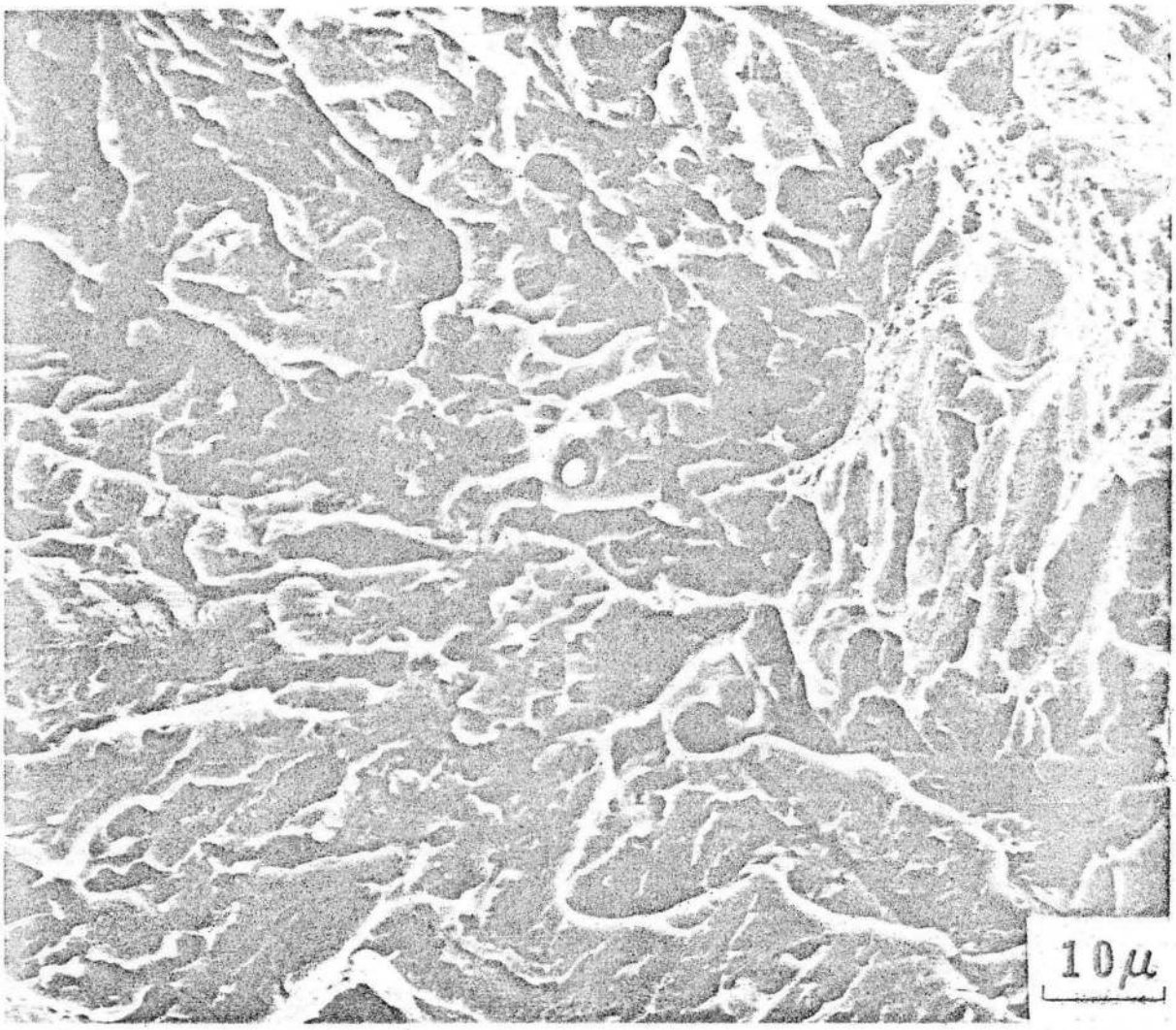

XBB 739-5586

Fig. 11

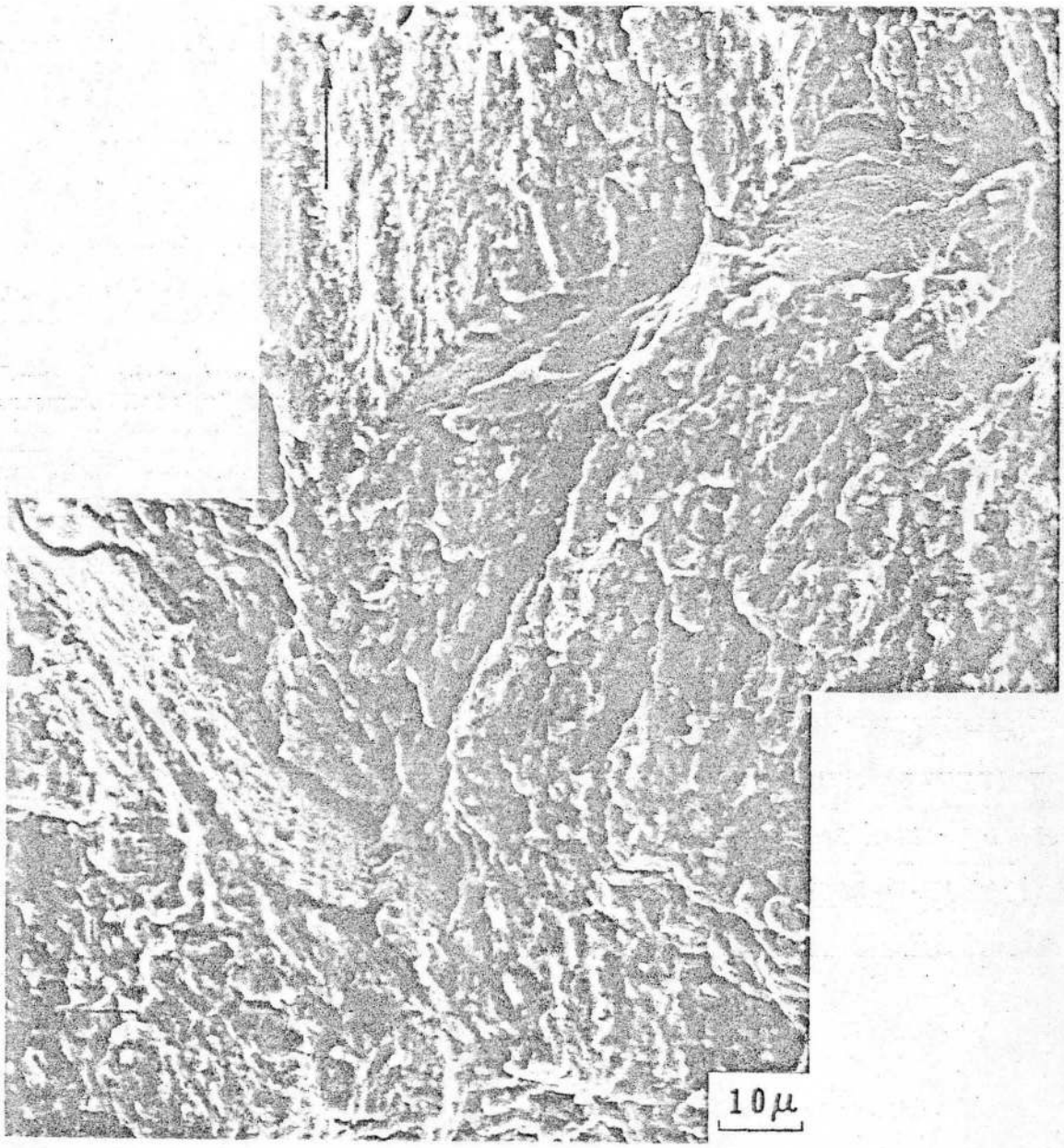

XBB 739-5580

Fig. 12

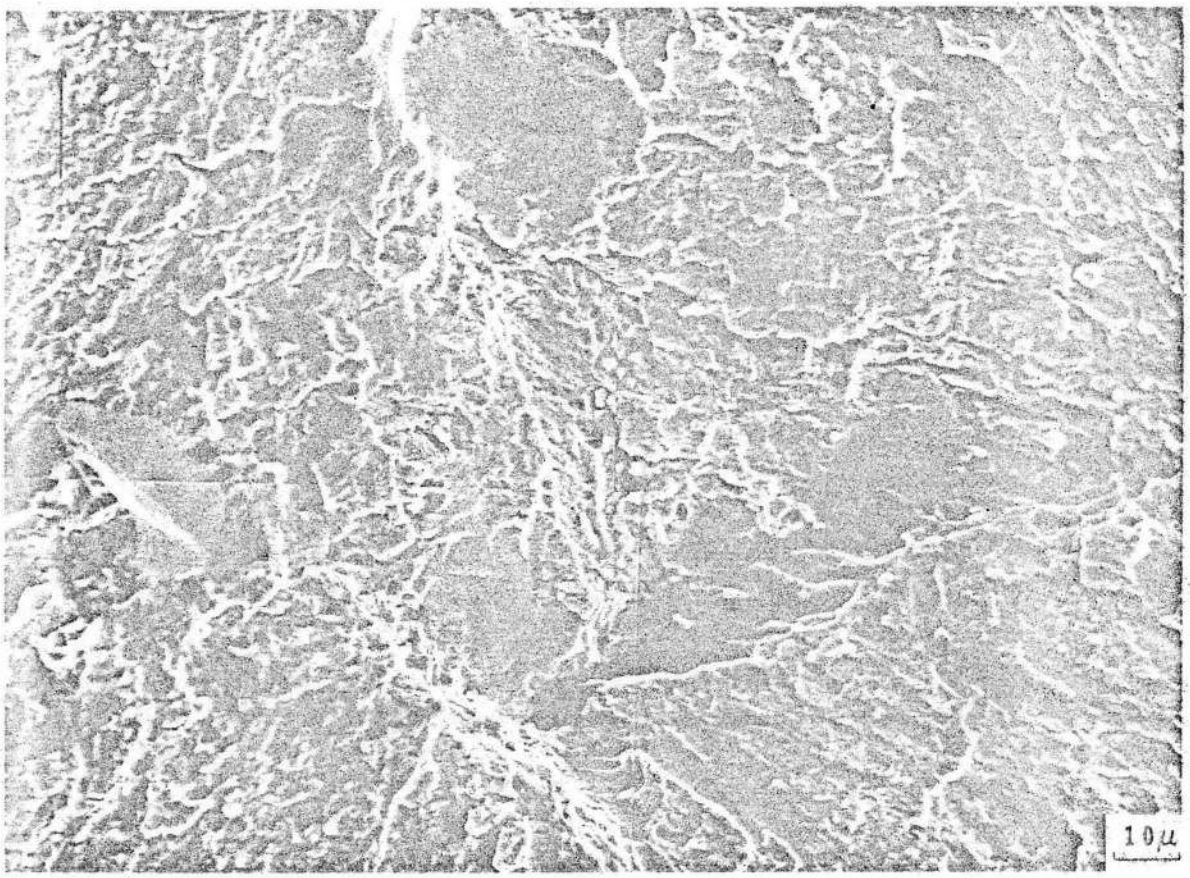

XBB 739-5582

Fig. 13

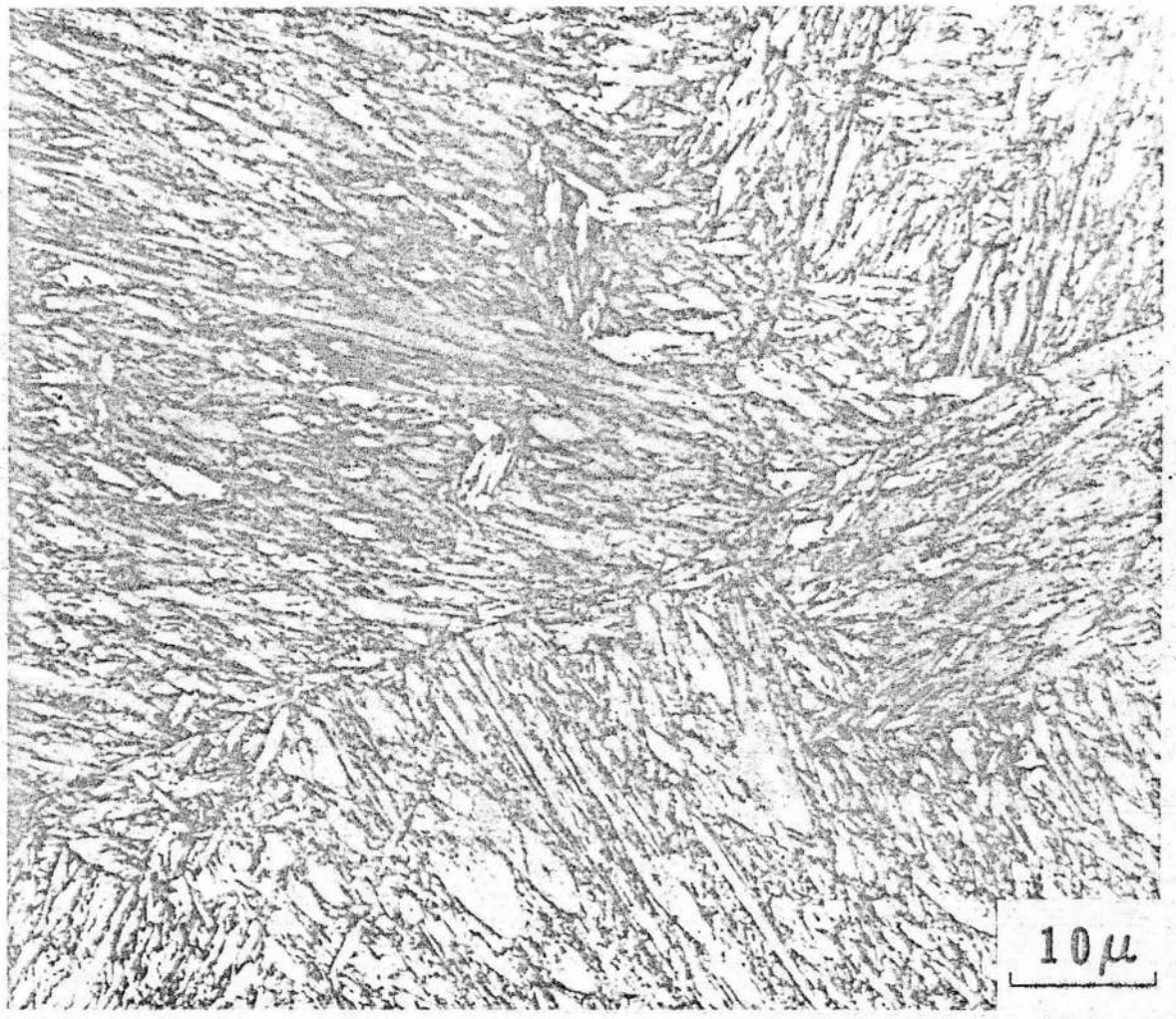

XBB 739-5585

Fig. 14

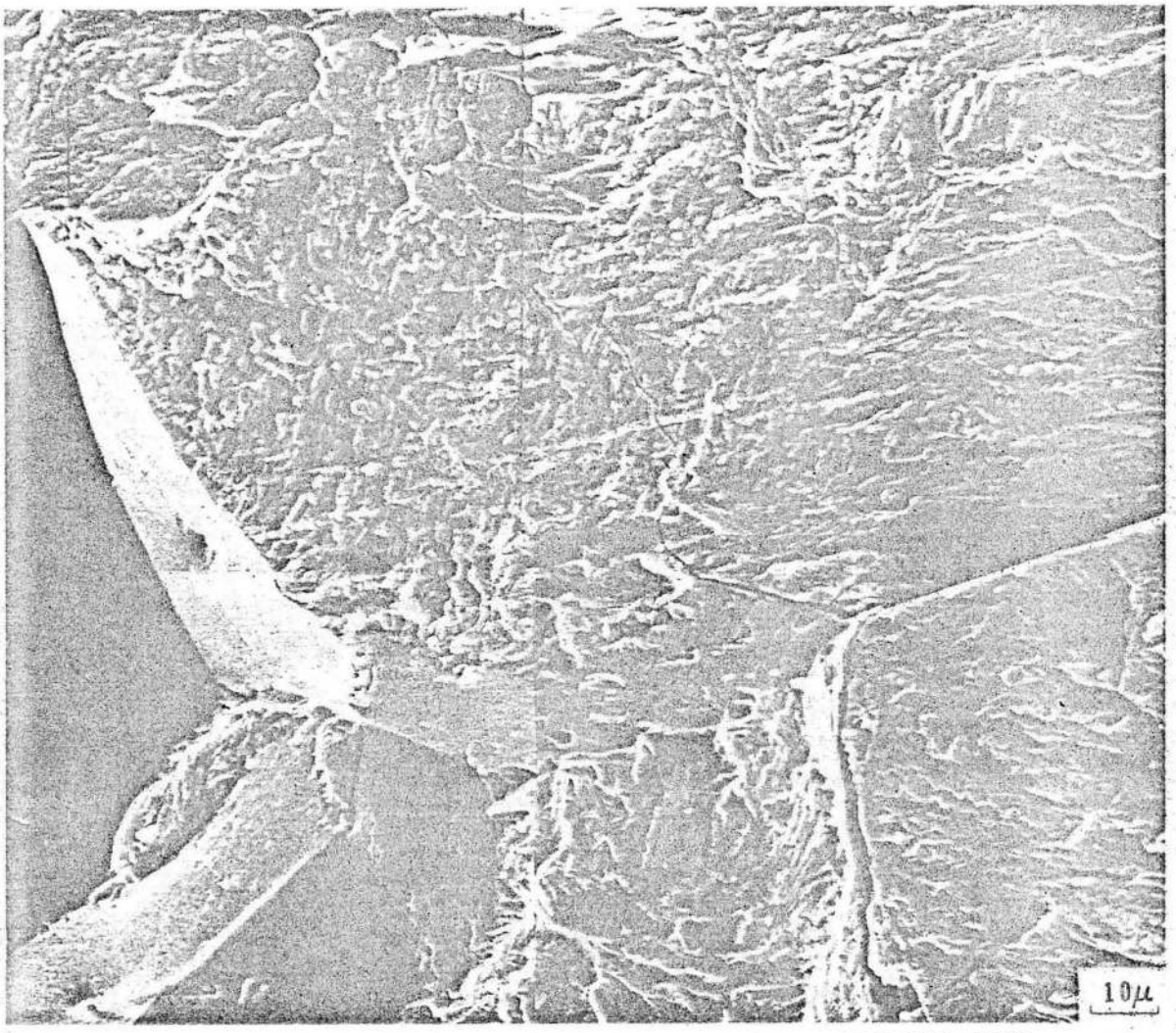

XBB 739-5583

Fig. 15

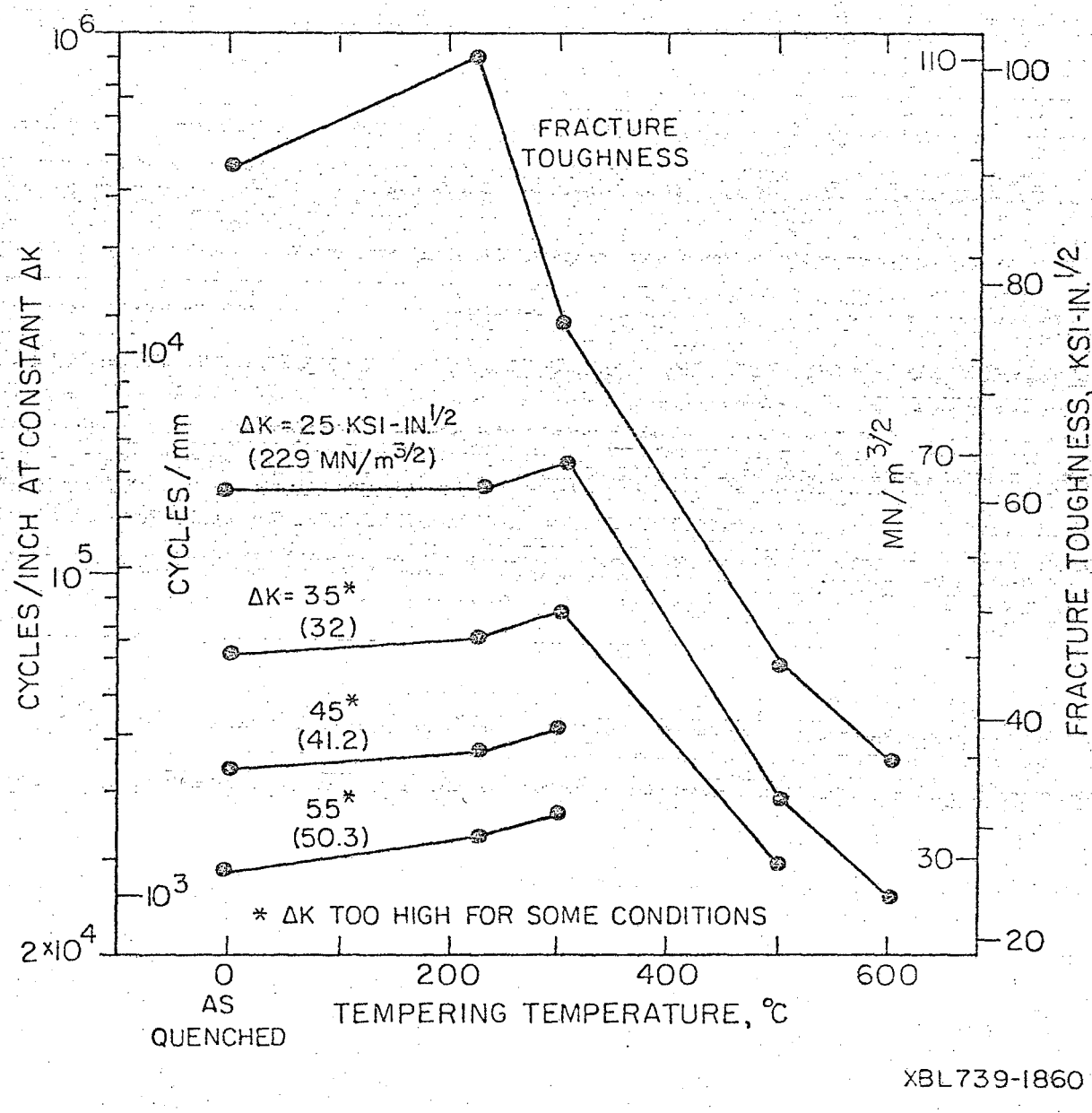
CYCLES/INCH AT CONSTANT ΔK
CYCLES/mm
FRACTURE TOUGHNESS
ΔK = 25 KSI-IN.1/2
(229 MN/m3/2)
ΔK = 35*
(32)
45*
(41.2)
55*
(50.3)
* ΔK TOO HIGH FOR SOME CONDITIONS
MN/m3/2
FRACTURE TOUGHNESS, KSI-IN.1/2
AS QUENCHED
TEMPERING TEMPERATURE, °C
XBL739-1860

Fig. 16

TECHNICAL INFORMATION DIVISION
LAWRENCE BERKELEY LABORATORY
UNIVERSITY OF CALIFORNIA
BERKELEY, CALIFORNIA 94720